CERN-ACC-NOTE-2020-0058

24 November 2020
ninad.chitnis@cern.ch

Study of the Effect of Detuning Impedance on Beam Stability

Ninad Chitnis Carlo Zannini Nicolas Mounet Giovanni Rumolo
CERN, CH-1211 Geneva, Switzerland

Keywords: SPS, detuning impedance, chromaticity, TMCI threshold, wake fields

Summary

The impact of the detuning impedance on the stability of a particle beam is a relatively less studied phenomenon compared to the usual case of considering only the driving impedance. This report tries to explore the area of the detuning impedance with a specific focus on the SPS. Different studies were carried to examine the effect and some key findings were made. The analytical model for two macroparticles (developed for the case of zero chromaticity) was confirmed with simulations. The dependence of the stabilising or destabilising effect of detuning on the second harmonic voltage was observed implying that the effect depends on the actual particle distribution. A Vlasov solver was used to verify the results of particle tracking simulations. The effect of non-linearities and higher order chromaticities was also studied. It was found that these effects have a significant impact on the TMCI threshold along with the detuning impedance. Finally, an analytical model was developed for observing the bunch by bunch tunes with multiple rigid bunches in presence of wakes and the results were compared with similar simulations.

Contents

1 Introduction

As a particle beam propagates through a particle accelerator, it interacts electromagnetically with the surrounding accelerator components. This leads to the creation of electromagnetic fields that are generated by the beam itself. Beam instabilities can emerge from strong enough self-generated fields. The strength of such interactions between the beam particles and their surroundings is characterised by the impedances (in the frequency domain) and the corresponding time domain representation called wake fields, of the accelerator components. The study of the effects of these impedances is crucial to the study of coherent beam instabilities. [1]

Such interactions act differently in the transverse plane or longitudinal plane. The effect of impedances in the longitudinal plane is outside the scope of this report. The impedances in the transverse plane are further classified into driving (also referred to as dipolar) impedance and detuning (also referred to as quadrupolar) impedance. While the driving impedance is a well-studied phenomenon, the effect of the detuning impedance is relatively less known. As machine performance is pushed higher, it becomes necessary to study the effects of all phenomena and their interplay with each other [2, 3].

The effects of the detuning impedance was recently reviewed in Ref. [4], for the case of a single bunch with zero chromaticity, where four approaches were compared. The simplest case of the two particle model is taken as the starting point for the studies detailed in this report. It is also worth mentioning that the effect of the detuning impedance on a coasting-beam was also recently studied, revealing a new kind of instability [5]. Thus, a two particle model is taken as the starting point for the studies detailed in this report. This report is divided into 5 following sections. First an explanation of the tools used for conducting the study as well as the naming conventions used is provided. This includes details of the impedances used. The next section covers the results obtained from particle tracking simulations. The third section consists of a comparison and benchmarking of the particle tracking approach with the results from a Vlasov solver based method. The fourth section describes the effect of other parameters such as the higher order chromaticities and non-linearities among others on the TMCI threshold. The fifth section contains an analytical approach for gauging the effect on multi-bunch beams, particularly the tune shift, followed by some concluding remarks.

2 Tools Used

For the macroparticle tracking simulations, PyHEADTAIL [6] was used. PyHEADTAIL is a Python based simulation tool developed in house at CERN and available at the link in Ref. [7]. It also provides different classes of impedances. Three of the available classes were used for the study. The impedances used were: a thick resistive wall, a broadband resonator and impedance generated from wake data in a pre-defined table representing the SPS impedance model. The wake table for the SPS was generated from scripts available at the CERN impedance repository [8]. The impedance classes take certain parameters as the input along with Yokoya factors to define the wake fields. Particle tracking being time domain, the impedances are defined in terms of wakes. The exact parameters used for these

classes are given in Appendix A. In all the simulations, the machine defined is the SPS with Q-20 optics. In case results with different optics are presented, the specific optics under consideration will be mentioned.

For the resistive wall and broadband resonator impedances, a parameter ρ is used. This parameter is defined as $\rho = \frac{k_Q}{k_D}$ where $k_Q \equiv$ quadrupolar or detuning wake and $k_D \equiv$ dipolar or driving wake. In all the studies changing value of ρ always implies change in k_Q. In the case of impedance from the real SPS model, 2 scenarios are considered. One is with only driving wake from the SPS wake table and the other is with both driving and detuning wakes.

EDELPHI, a Vlasov solver approach by G. Iadarola at CERN [9] has also been used for verifying the results obtained from PyHEADTAIL. Vlasov solvers are an alternative to particle tracking simulations. They are based on the Vlasov equation and use perturbation theory to solve the equation in mode domain [10].

For data analysis and plotting of graphs, MATLAB R2019 has been used. An exponential fit is obtained from MATLAB by fitting linearly, the log of the section wise fft of the turn by turn data as suggested by [11]. A direct exponential fit is also used and the results obtained from the best of both the fits are displayed.

The analytical model has been completely developed in python and uses a multi-turn wake file instead of single turn wakes. Scipy is used extensively in the generation of the matrices required by the model. The tunes are obtained from Harpy, a harmonic analysis tool also developed at CERN using python and available at the link in Ref. [12].

3 Macroparticle Tracking Simulations

Macroparticle tracking is a well known way to observe the beam parameters turn by turn. The parameters associated with each macroparticle were stored for each turn and the mean of the particles was observed. An example of a plot of the raw data obtained can be seen in Fig. 1. The plot in Fig. 1a is for zero chromaticity and shows a stable beam as expected for operation in the Head-Tail regime. At non-zero chromaticities, an exponentially increasing beam is expected as seen in Fig. 1b.

For observing the effect of the detuning impedance at non-zero chromaticities, the growth rate with different values of detuning wake was plotted against chromaticity, the results of which are displayed in Fig. 2 for two macroparticles. The plot for operation in the head-tail regime can be seen in Fig. 2a and it reveals only a minor effect of the detuning impedance. The general shape of the curve matches the predictions of [13] where an analytical approach including both the detuning impedance and chromaticity in the two particle model is proposed to study the effect of the damper for suppression of transverse instabilities. As Ref. [13] did not focus on the effect of the detuning impedance, it makes a direct comparison difficult.

However, when either the beam intensity or the driving impedance is increased to reach the TMCI regime, the effect of the detuning impedance is no longer subtle. Particularly for zero chromaticity, the effect is strongly dependent on the value of ρ as is apparent from Fig. 2b which shows the growth rate for a larger range of chromaticity. To put it in words, for $|\rho| \geq 1$, the beam is always stable at zero chromaticity while for $|\rho| \leq 1$, the beam is

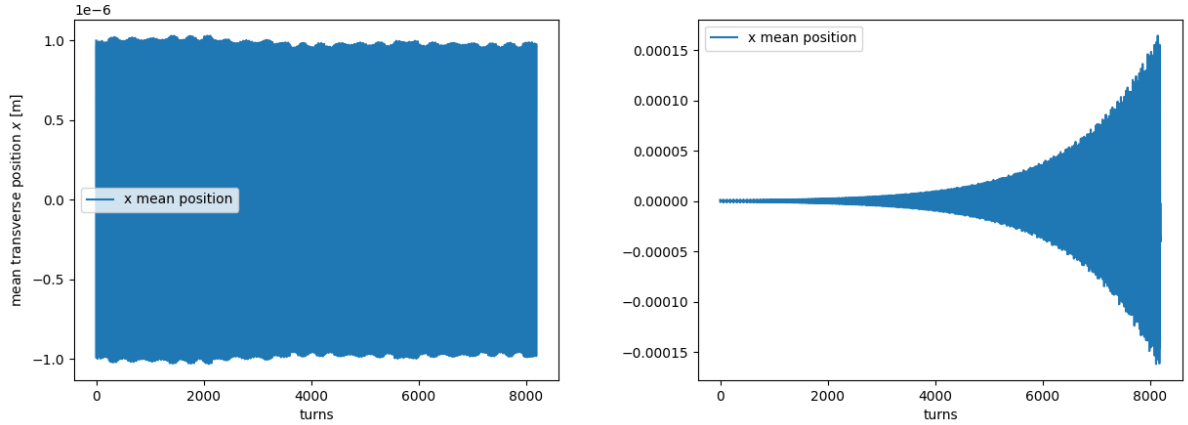

(a) Stable beam at zero chromaticity

(b) Unstable beam at non-zero chromaticity

Figure 1: Plot of mean of particle positions against number of turns.

more stable than in absence of the detuning impedance. This confirms Ref. [4]. Even for low non-zero chromaticities, the detuning impedance has a strong stabilising effect. Only for higher chromaticities it is observed that the growth rate is higher for some high values of ρ than for $\rho = 0$. An example of this can be seen for $|\rho| = 1.5$ for a chromaticity of ± 1.

After observing the effect on an academic two particle model, the tracking simulations were repeated by considering a more realsitic beam with 5×10^5 macroparticles. The plot of the growth rate in $1/turns$ can be seen in Fig. 3 for different values of ρ with linear and non-linear synchrotron motion considered in the head-tail regime. From Fig. 3a, which considers linear synchrotron motion, it can be seen that the detuning impedance is always stabilising. But when non-linear synchrotron motion is considered, the effect is strongly dependent on the sign of ρ, as seen in Fig. 3b. For negative chromaticity, a mild stabilising effect is always observed. However the stabilisation is too low to be observed practicaly and the growth rate can be estimated only using the driving impedance as already predicted in [14]. For a chromaticity in the range of 0 to 0.6, it can be said that for $\rho < 0$, there is a destabilising effect while for $\rho > 0$ there is a stabilising effect. On the other hand, no clear trend is observed for chromaticities higher than 0.6.

A more illustrative example of such an effect can be seen when considering a flat chamber as seen in Fig. 4. The behaviour seen is as expected from Fig. 3. A chromaticity sweep from -1 to 1 is plotted in Fig. 4a for both the X and Y planes. For a flat chamber, the X plane has $\rho = -1$ and the Y plane has $\rho = 0.5$ with the factor ρ referred to the value of the driving impedance in the respective planes. The value of the detuning impedance itself is equal and opposite in the two planes. Accordingly, a stabilising effect should be seen in the Y plane and a destabilising effect in the X plane. It should be noted that normally, in absence of the detuning impedance, the X plane is more stable than the Y plane. But due to this particular effect on mode 1, a situation where the Y plane is more stable than the X plane is obtained. This can be seen more clearly in Fig. 4b where a plot of only positive chromaticity is shown.

This effect however, is strongly seen only in the absence of the second harmonic RF

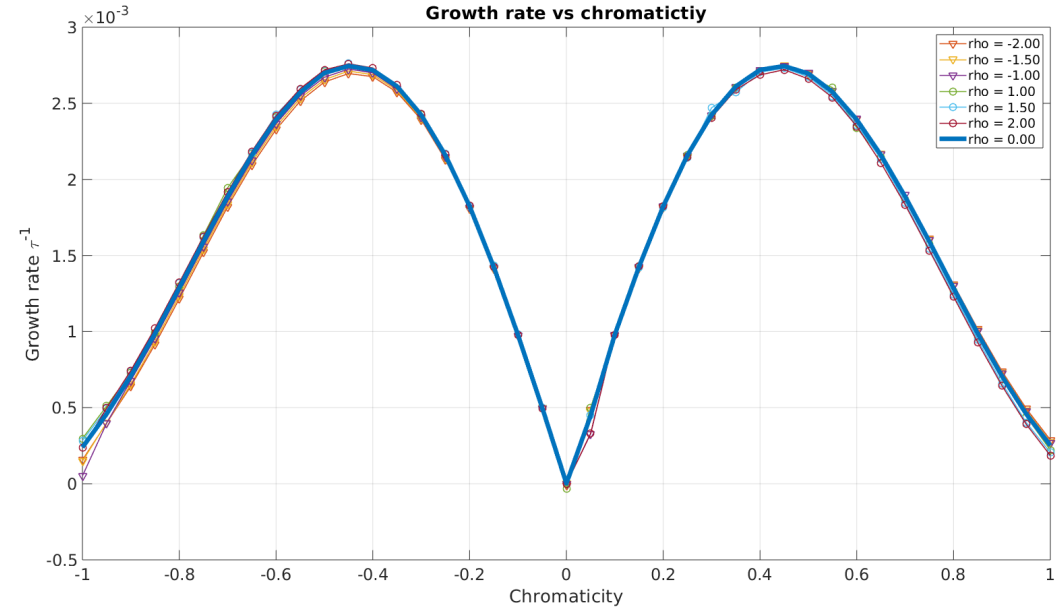

(a) Head-tail regime.

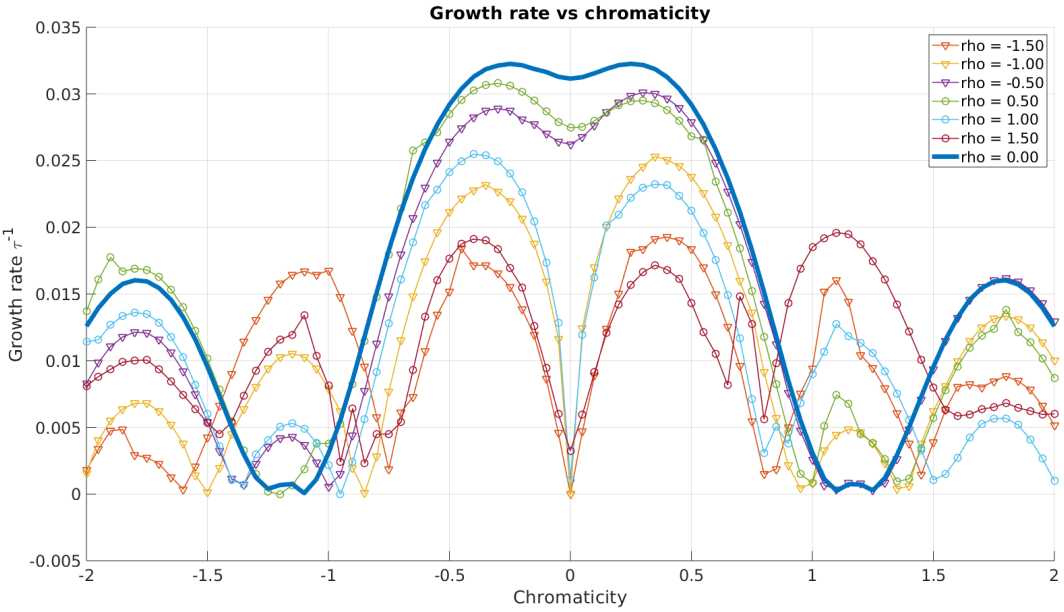

(b) TMCI regime.

Figure 2: Growth rate in 1/turns against chromaticity for different values of ρ for two macroparticles.

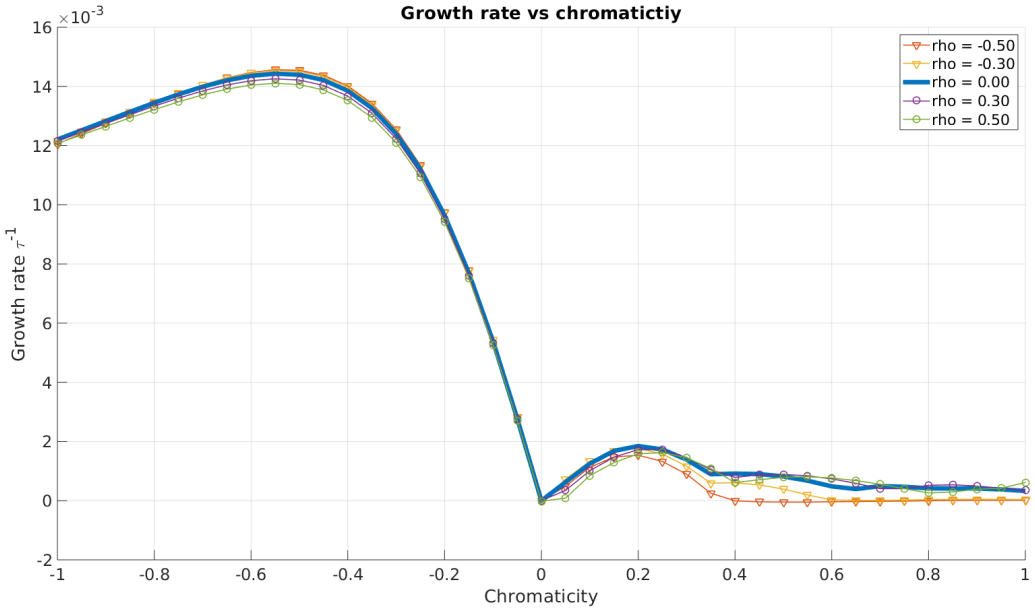

(a) Linear synchrotron motion.

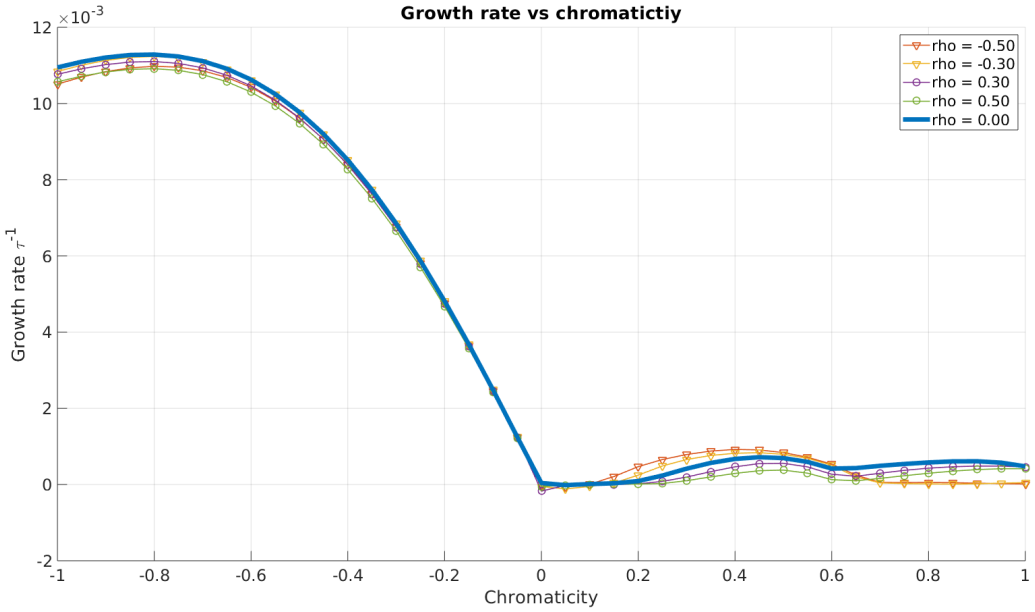

(b) Non-linear synchrotron motion with a single harmonic.

Figure 3: Growth rate in 1/turns against chromaticity for 5×10^5 macroparticles for different values of ρ.

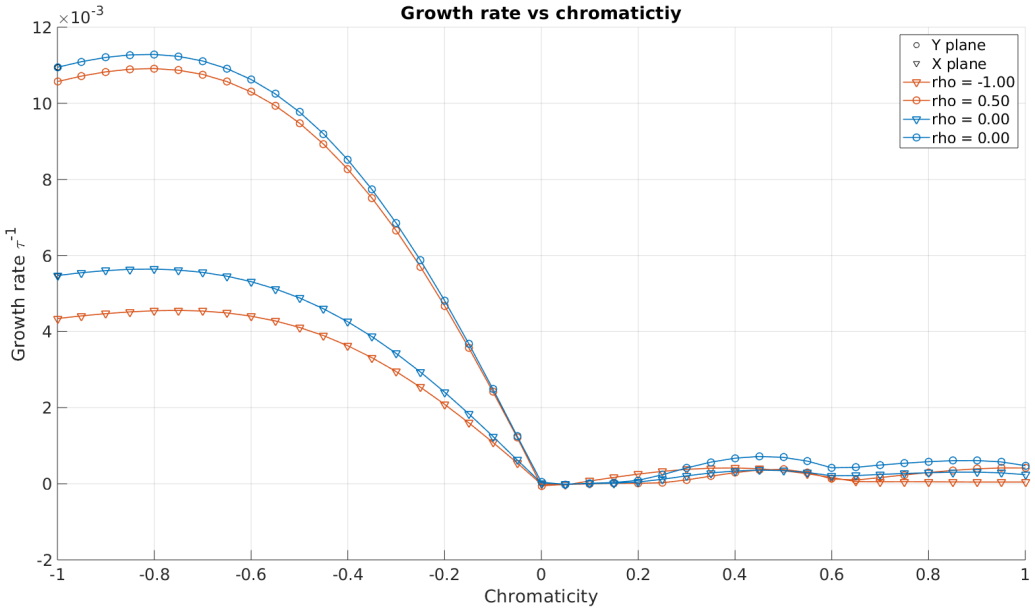

(a) Full chromaticity sweep from -1 to 1.

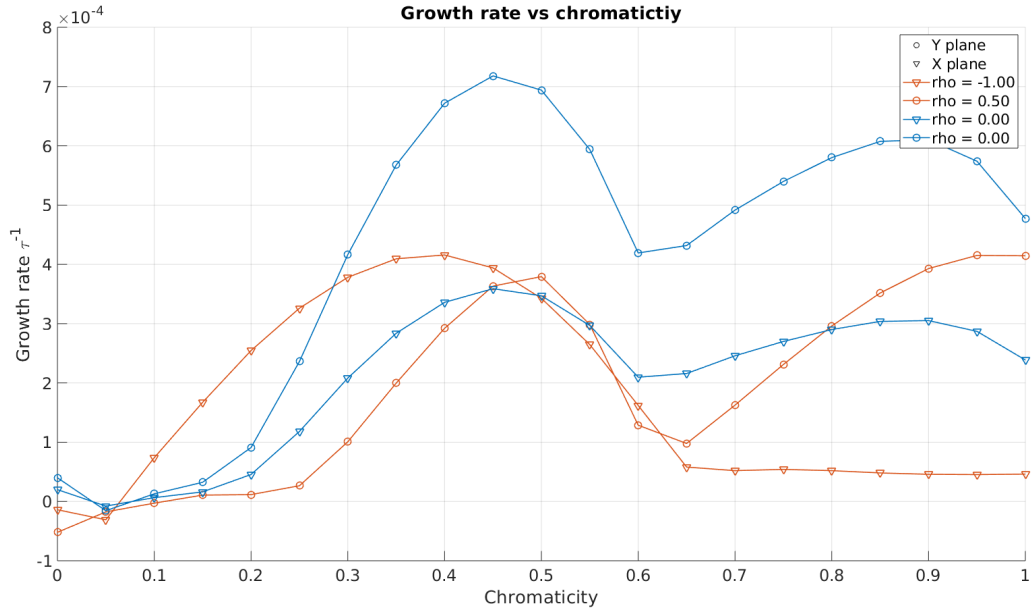

(b) Positive chromaticity sweep from 0 to 1.

Figure 4: Growth rate in 1/turns against chromaticity for a flat chamber with 5e5 macro-particles.

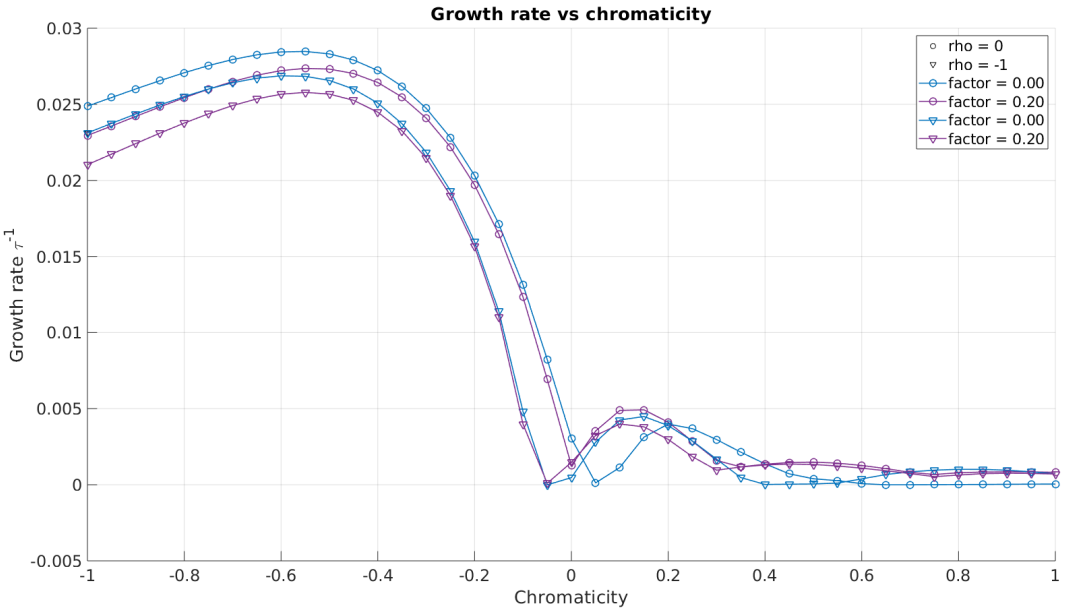

Figure 5: Growth rate in 1/turns against chromaticity for 5e5 macroparticles for two values of second harmonic. The variable factor represents the factor by which the first harmonic is multiplied to obtain the second harmonic.

voltage. When the second harmonic RF voltage is gradually increased as a percentage of the first harmonic, the destabilising effect reduces and eventually vanishes completely to result in a stabilising effect irrespective of the sign of ρ. A plot of the growth rate versus chromaticity for two different values of second harmonic can be seen in Fig. 5. The figure shows two curves each (with $\rho = 0$ and $\rho = -1$) for two values of the second harmonic. The parameter $factor$ represents the factor by which the first harmonic is multiplied to obtain the second harmonic. The circles represent no second harmonic while the triangles represent a second harmonic RF voltage which is 20% of the first harmonic voltage. It can be clearly seen in mode 1 that for $factor = 0.20$, there is a stabilising effect while for $factor = 0$, a destabilising effect is observed.

In the course of this work, it was noted that for some value of the detuning impedance, an instability is observed at zero chromaticity. Hence studies were also carried out to find the effect of the detuning impedance on the TMCI threshold. The plots for this study can be seen in Fig. 6 for three different types of impedances. In the Fig. 6a, a resistive wall impedance is considered. It can be seen that for high negative values of the detuning impedance, the threshold vanishes and there is a steady rise in the growth rate. For low negative values, the threshold is increased. For positive values of the detuning impedance, the threshold increases till $\rho = 1$, and decreases thereafter. The most striking effect of the detuning impedance is seen with a broadband resonator as in Fig. 6b. There is a clear increase in the threshold with negative values of ρ and a decrease in the threshold for positive values. The same sweep is then run on a realistic SPS impedance model. Only the case in presence and absence of the detuning impedance is considered for a faithful comparison and to keep the analysis realistic. While the absolute threshold is increased for both the horizontal and vertical planes due to

the detuning impedance, from Fig. 6c it can be noticed that at certain lower intensities the beam is more unstable in presence of the detuning impedance than in its absence.

4 Vlasov Solver Based Simulations

In this section, the results from Sec. 3 have been compared to the results obtained from the EDELPHI solver [9]. This served the purpose of verifying the results and also benchmarking the EDELPHI solver.

As a first step, chromaticity sweep for the resistive wall with flat chamber conditions similar to that seen in Fig. 4 was repeated with EDELPHI. A direct comparison of the results obtained from the two tools can be seen in Fig. 7 and is found to be in good agreement, particularly for negative chromaticity. Some discrepancy in the growth rate values is observed for positive chromaticty though the general shape of the curve is similar. An intensity sweep with the SPS impedance model was also carried to find the TMCI threshold. The result was expected to be similar to Fig. 6c. The result obtained from EDELPHI can be seen in Fig. 8. While the two tools agree well up to a growth of 500 s^{-1}, beyond that they begin to diverge though the general shape of the plot is still similar. This disparity can be attributed to the fact that at higher growth rates obtaining accurate values from PyHEADTAIL is diffcult. The growth rate is obtained relatively directly from a Vlasov solver but it needs to be obtained from PyHEADTAIL data by fitting an exponential curve as explained in Sec. 2. This introduces a degree of uncertainty in the obtained fit for fast growing exponentials.

An advantage of using EDELPHI over PyHEADTAIL is the ability to obtain detailed tune analysis. Obtaining the tunes from PyHEADTAIL data is limited up to an arbitrary intensity close to where the first modes begin to couple. A plot of tunes obtained from PyHEADTAIL and EDELPHI for the X plane can be seen in Fig. 9 and for the Y plane in Fig. 10. From the figures the difference between the two tools is obvious and shows that EDELPHI allows observing a clear picture of the tune shift of each mode well above the intensity of the first mode coupling. It is also possible to observe the growth rates associated with each mode.

5 Effect of Machine Parameters

It is also important to study the effect of other dynamic beam properties such as emittance, linearity of synchrotron motion and machine properties such as higher order chromaticities on the TMCI threshold. For that reason, dual parameter sweeps were carried out with one parameter being the intensity. In this section, two studies will be detailed, one being a study of the effect of the longitudinal emittance and the other dealing with chromaticity.

The effect of longitudinal emittance in presence and absence of the detuning impedance for linear synchrotron motion can be seen in Fig. 11. The parameter varied during this study is the bunch length and the emittance was obtained as a function of the bunch length. From the plots it is clear that the detuning impedance has a greater effect at higher emittances, that is for longer bunches. Particularly, in the horizontal plane, it can be seen that for the intensity range considered, the threshold is not encountered, signifying that the detuning impedance has increased the threshold considerably. As part of the study, higher order

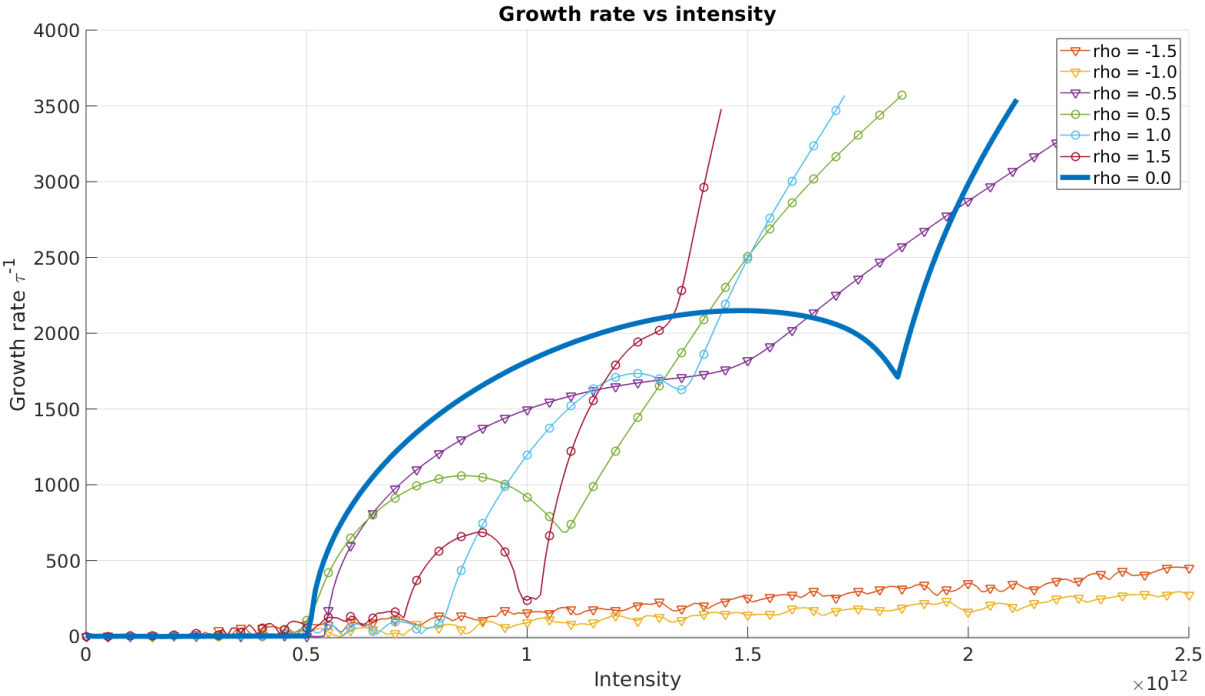

(a) Growth rate against intensity for resistive wall impedance.

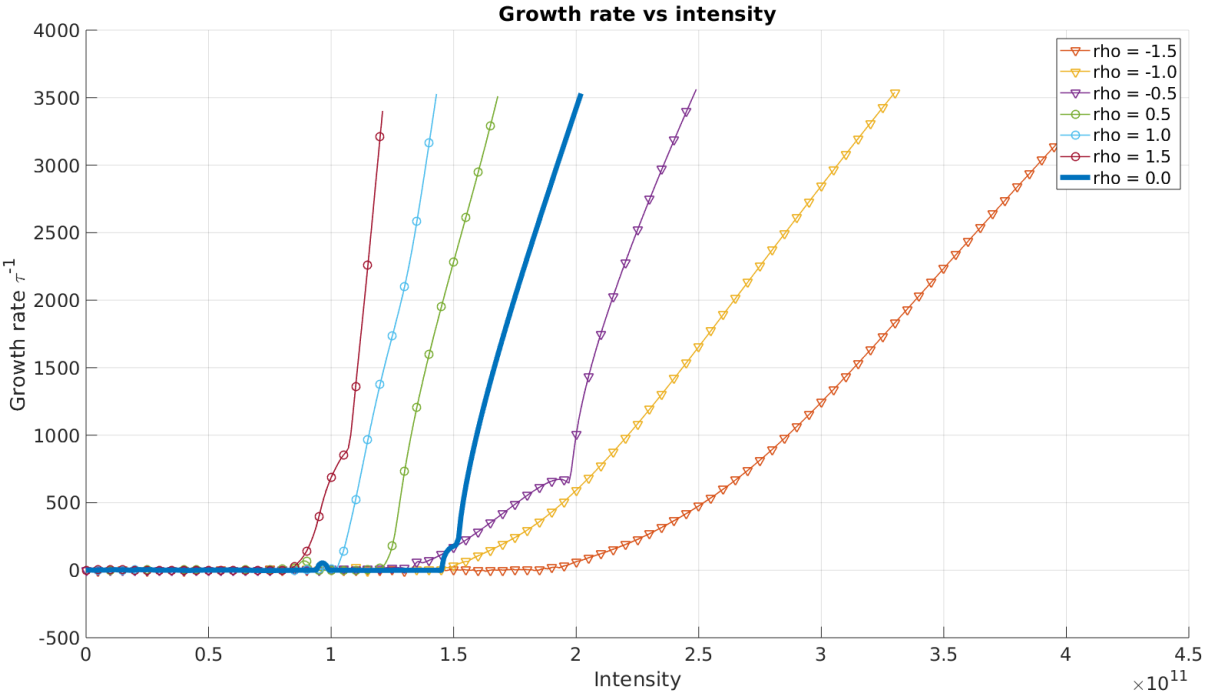

(b) Growth rate against intensity for broadband resonator.

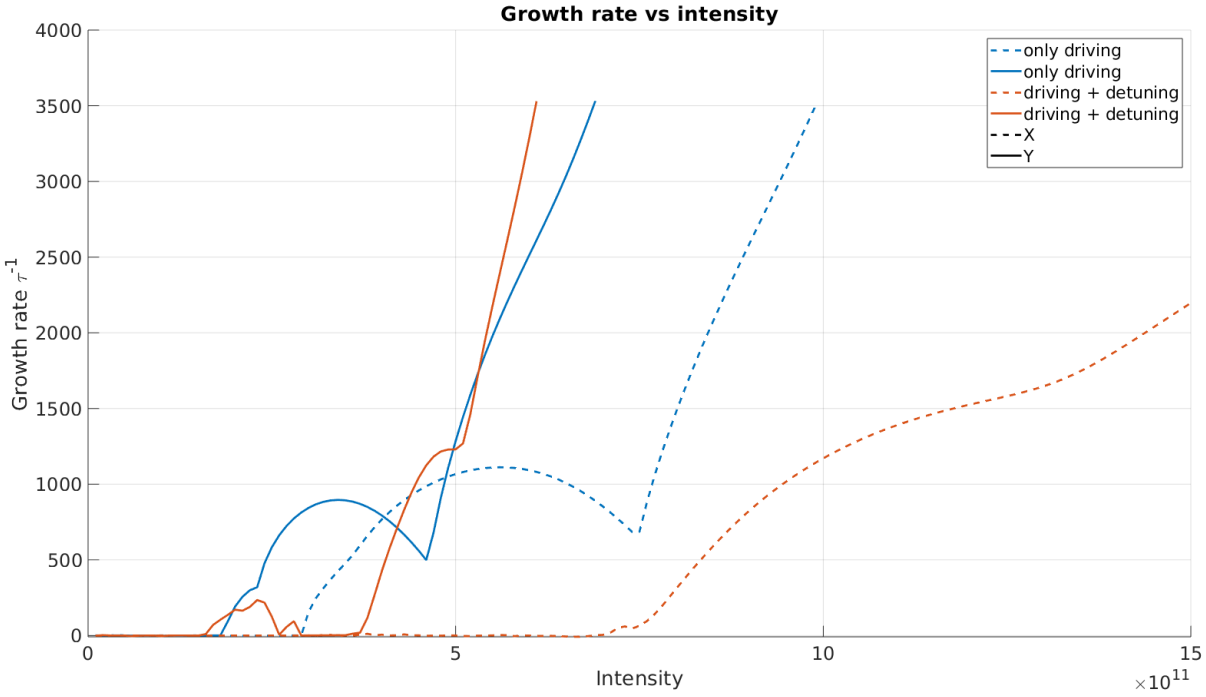

(c) Growth rate against intensity for real SPS wake model.

Figure 6: Growth rate in 1/s against intensity for different impedances.

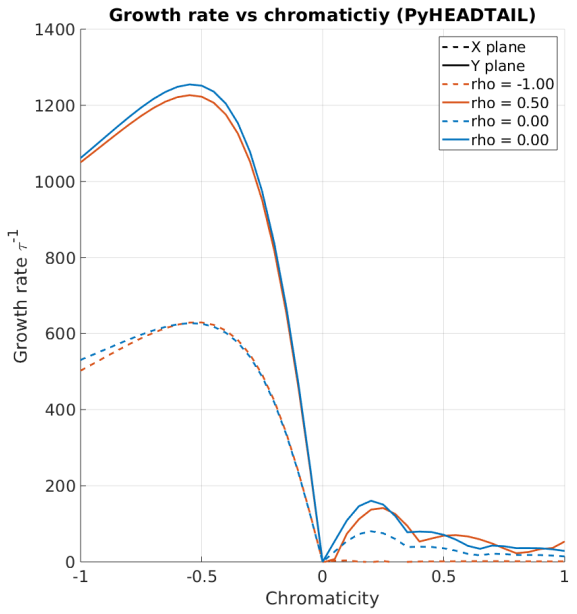

(a) Results from PyHEADTAIL.

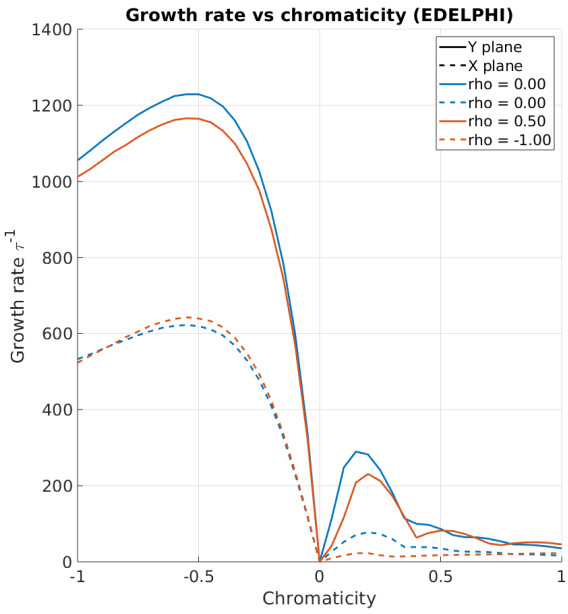

(b) Results from EDELPHI.

Figure 7: Growth rate in 1/s against chromaticity for a flat chamber using PyHEADTAIL and EDELPHI.

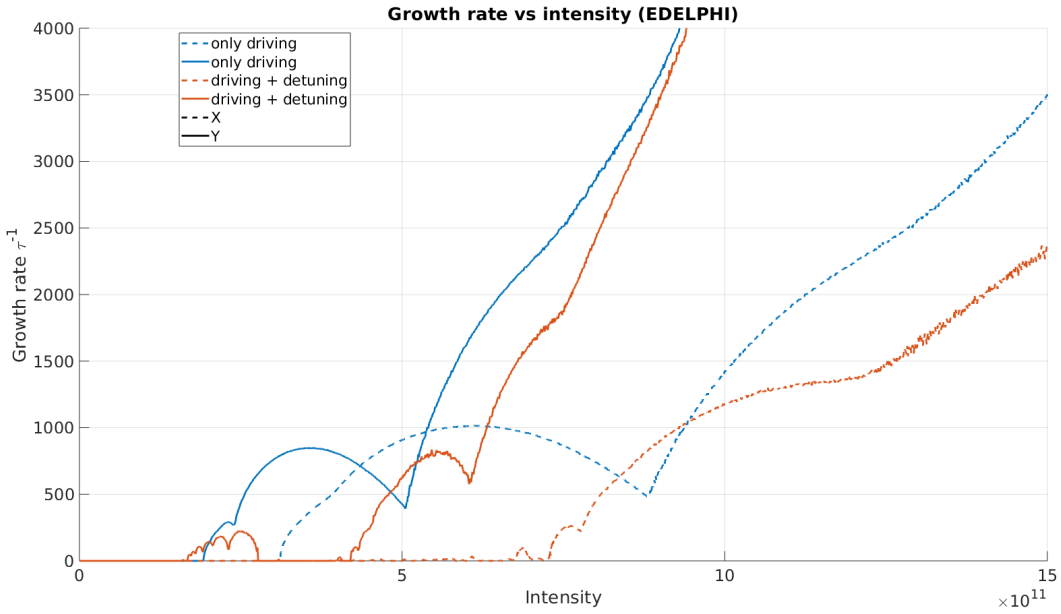

Figure 8: Growth rate in $1/s$ against intensity for the SPS impedance model obtained from EDELPHI.

chromaticities are gradually introduced. First, only non-linear synchrotron motion with two harmonics (the second harmonic being 15% of the first) and no higher order chromaticities is considered. The plot for this case can be seen in Fig. 12. Next, second order chromaticity effect is considered which can be seen in Fig. 13. As the last step, third order chromaticity is also introduced. The plots for this model can be seen in Fig. 14.

Such a gradual introduction of higher order effects allows decoupling of the results according to the conditions. From the figures, it is clear that while the detuning impedance always increases the threshold, the higher order chromaticities prove to be the limiting factor for the threshold. Of particular note, is the third order chromaticity which greatly destabilises the X plane while proves to beneficial for the Y plane.

An interesting study after observing these effects is to look at the variation in the threshold with chromaticity for different machine optics. The results for this study have been plotted in Figs. 15-17. From the results, it is clear that the detuning impedance does affect the threshold even with high chromaticity and has a stronger impact impact in the horizontal plane. It is also worth noting from the Figs. 15-17 that different optics are affected differently by chromaticity. At zero chromaticity, the TMCI threshold, both in presence and absence of the detuning impedance, is the lowest in Q-26 optics, followed by a slightly higher threshold in Q-22 optics and the highest among the three in Q-20 optics. At higher chromaticities, however, this situation is reversed due to the difference in the chromatic frequency shift for different optics with change in the chromaticity unit. The lowest threshold is displayed in Q-20 optics followed by Q-22 followed by the highest threshold in Q-26. From the same figures, it can be seen that the thresholds with different optics are approximately equal around a chromaticity factor of 0.4 for the Y plane and between 0.1 and 0.2 for the X plane.

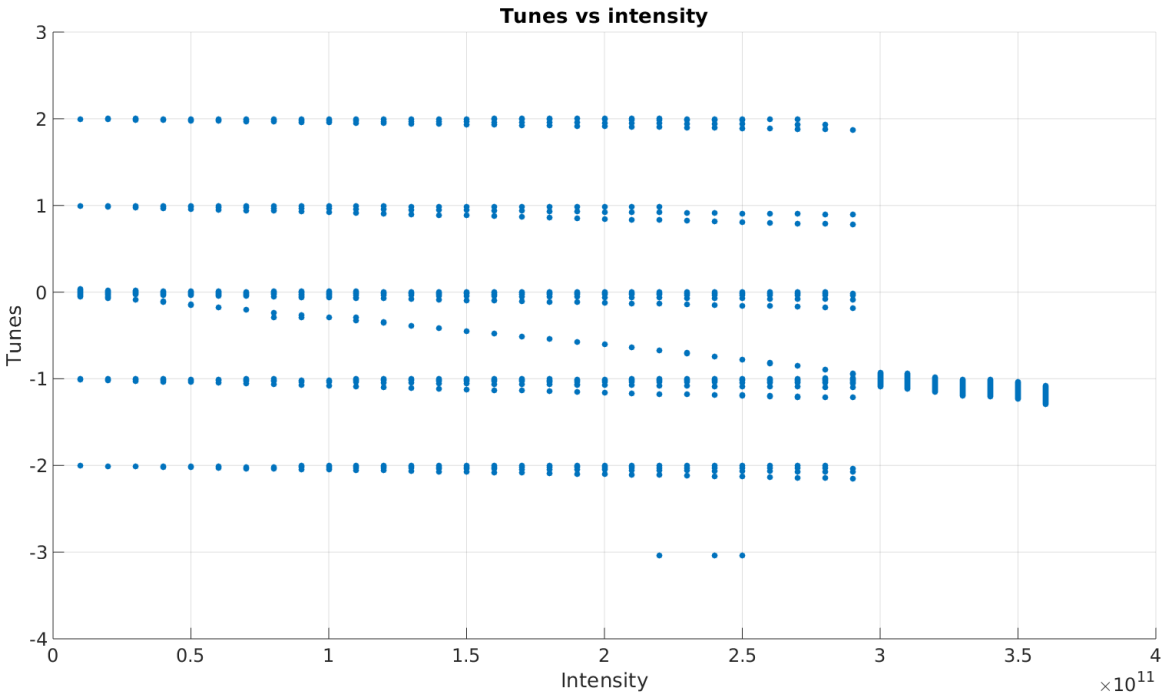

(a) Tunes against intensity without the detuning impedance from PyHEADTAIL.

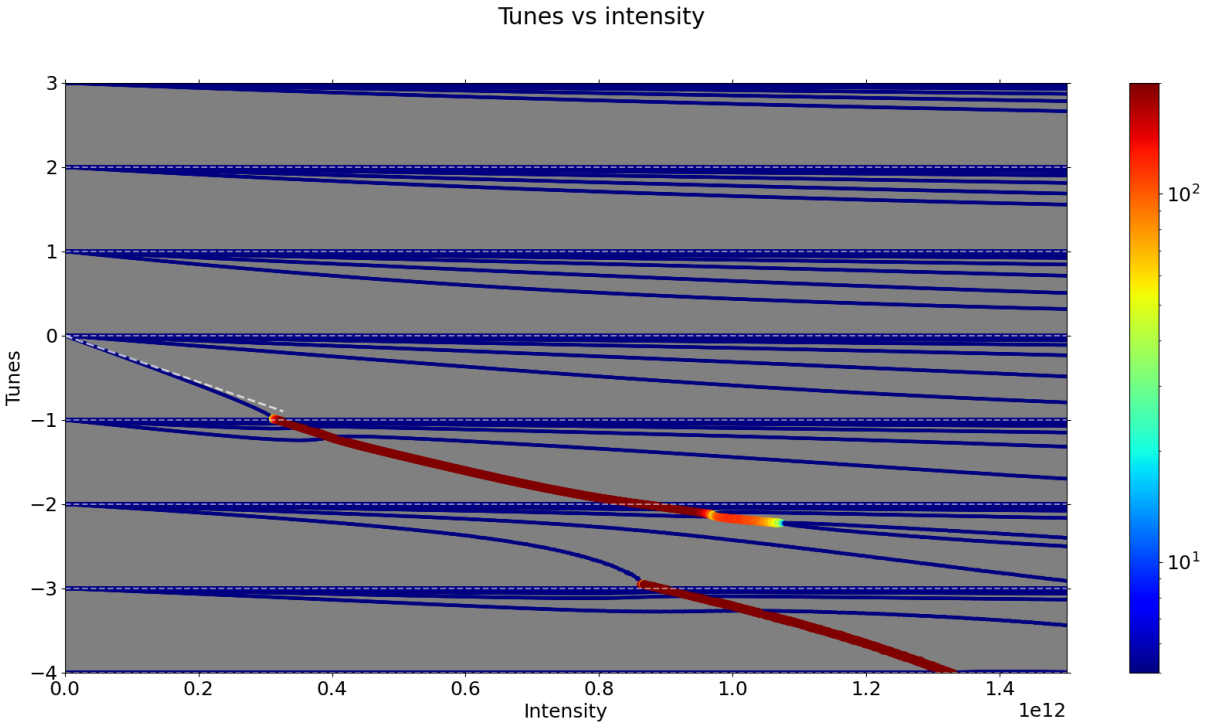

(b) Tunes against intensity without the detuning impedance from EDELPHI.

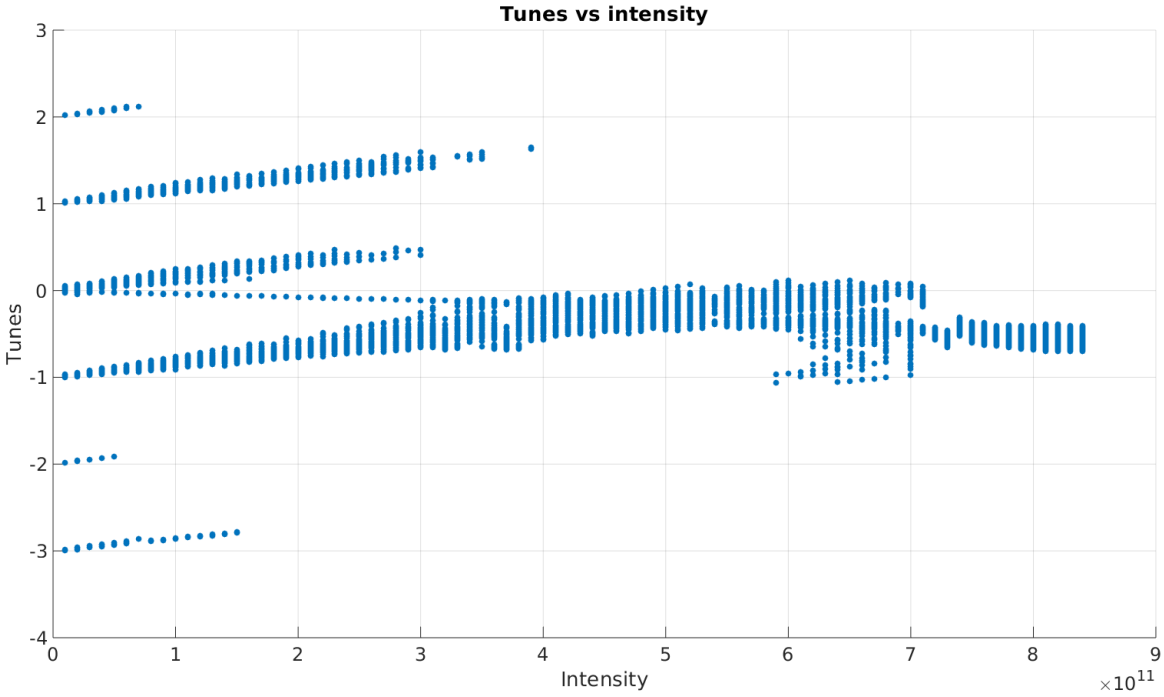

(c) Tunes against intensity with the detuning impedance from PyHEADTAIL.

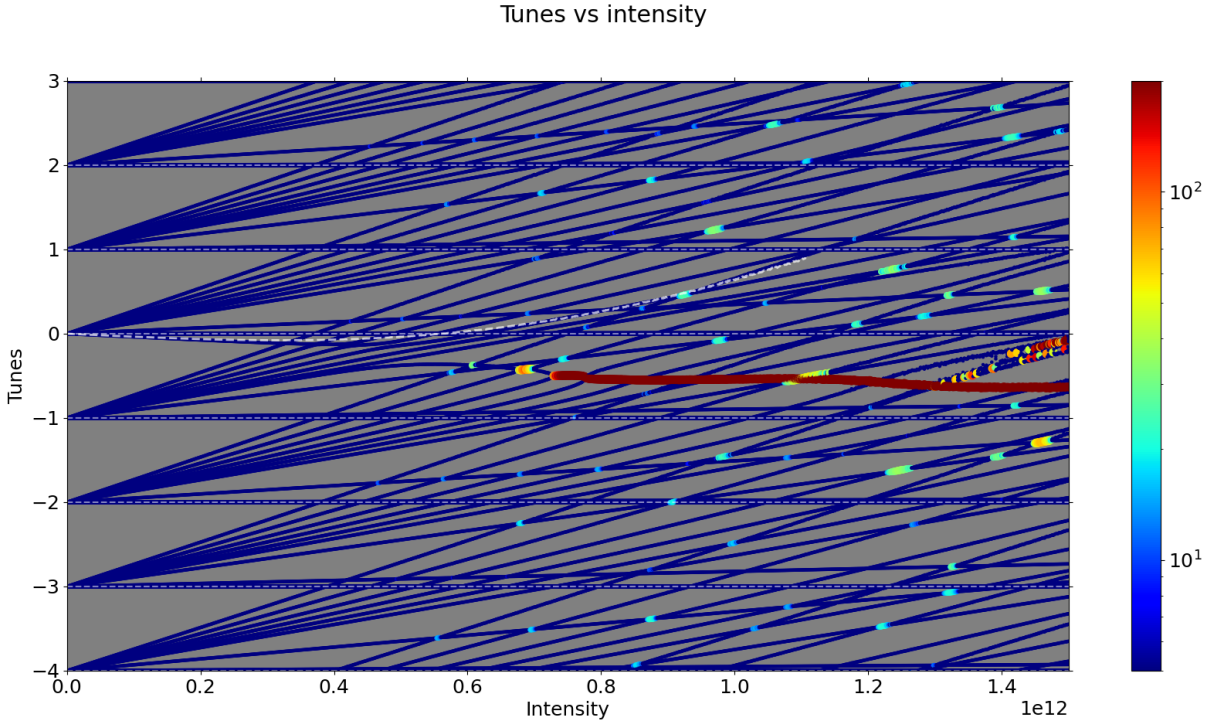

(d) Tunes against intensity with the detuning impedance from EDELPHI.

Figure 9: Tunes against intensity for the X plane.

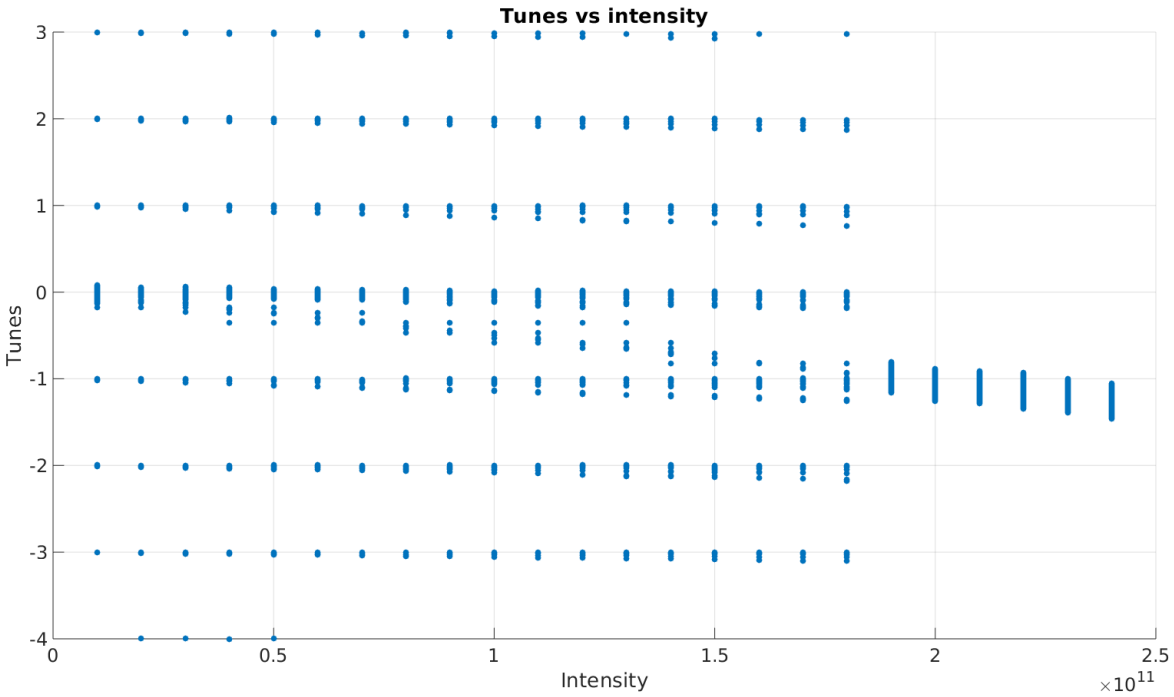

(a) Tunes against intensity without the detuning impedance from PyHEADTAIL.

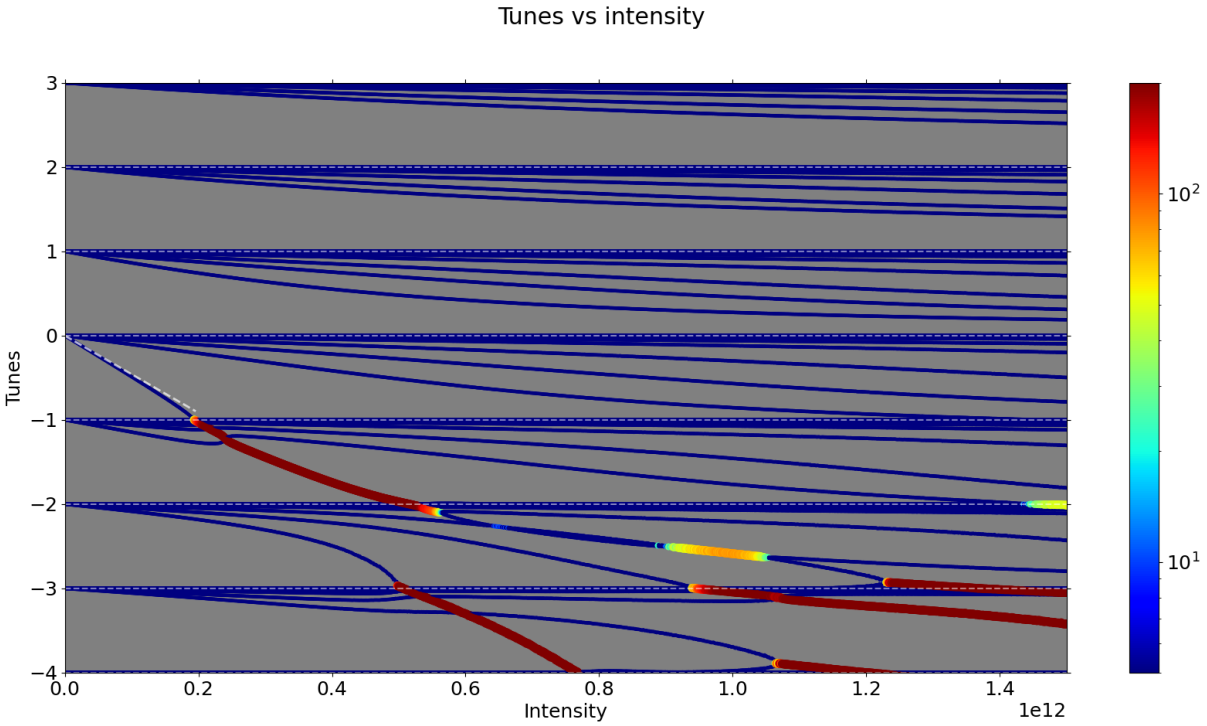

(b) Tunes against intensity without the detuning impedance from EDELPHI.

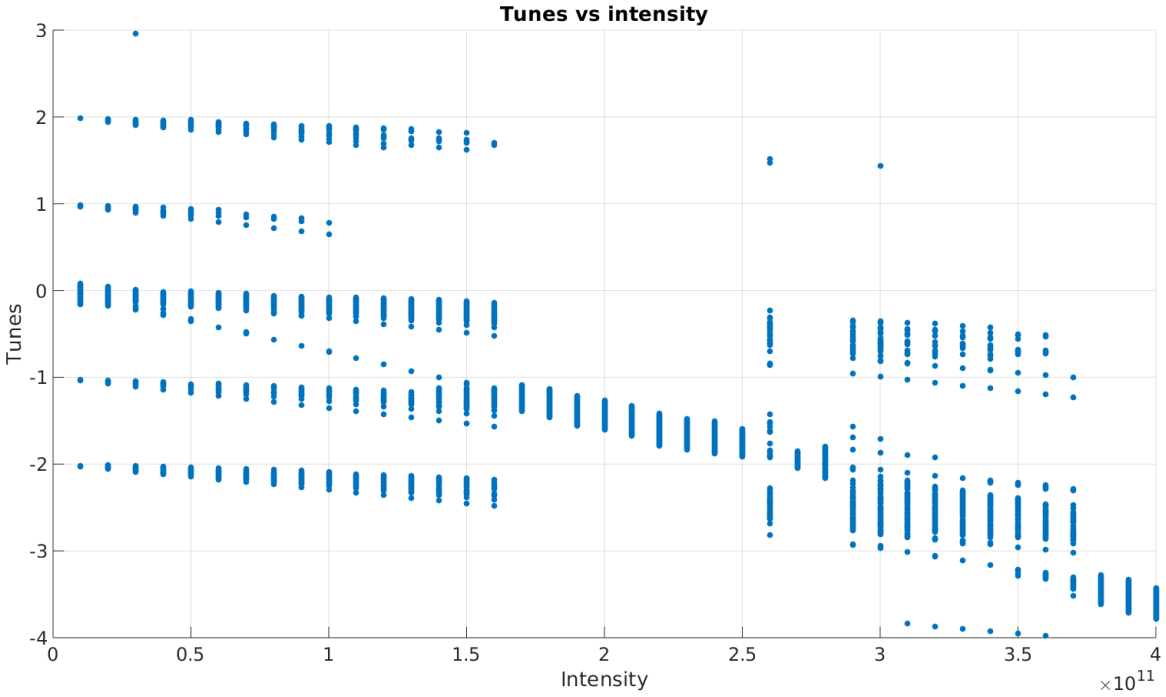

(c) Tunes against intensity with the detuning impedance from PyHEADTAIL.

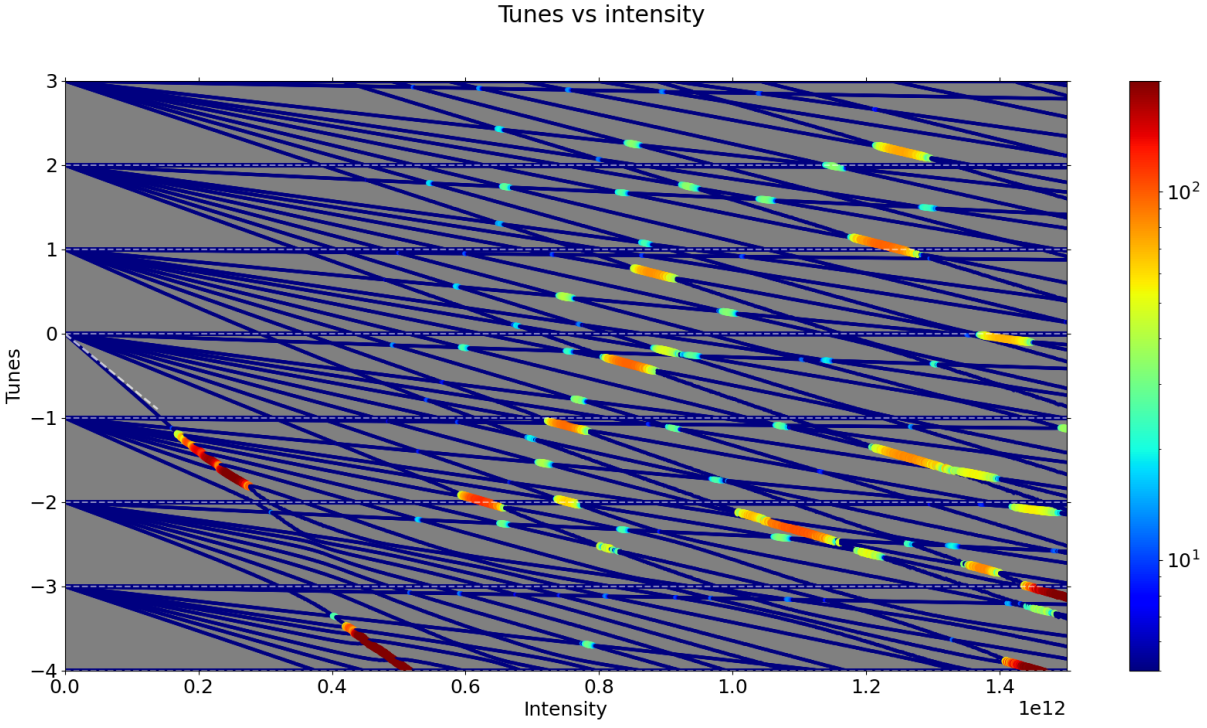

(d) Tunes against intensity with the detuning impedance from EDELPHI.

Figure 10: Tunes against intensity for the Y plane.

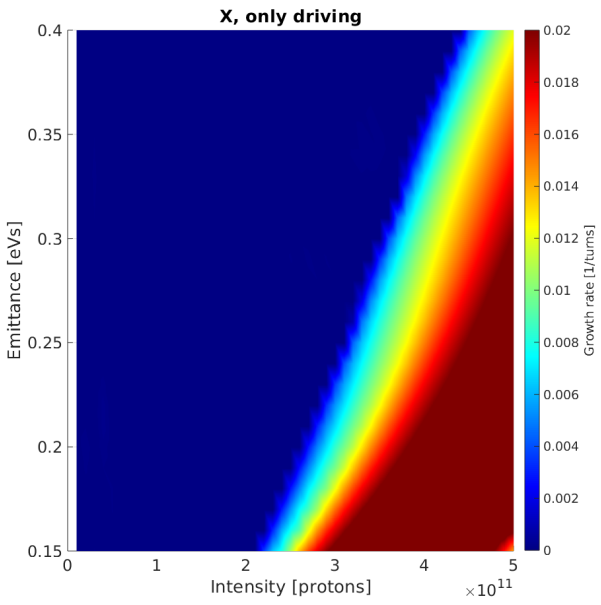

(a) X plane without the detuning impedance.

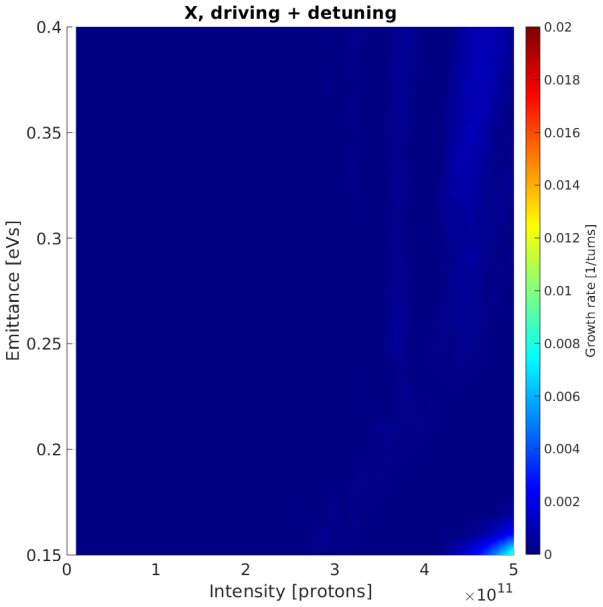

(b) X plane with the detuning impedance.

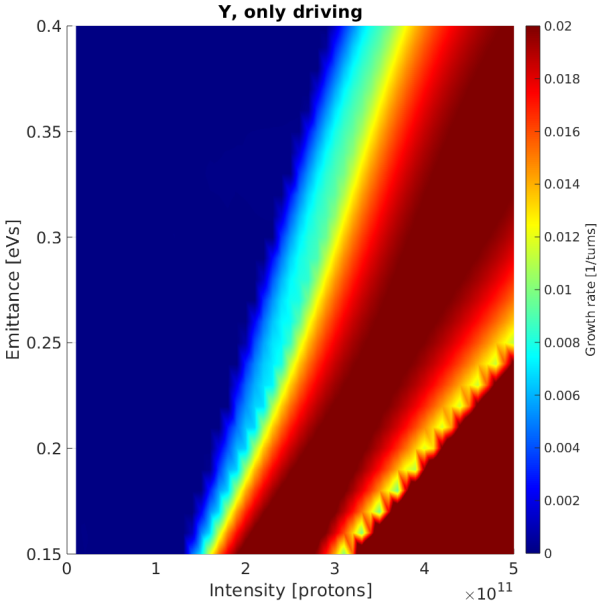

(c) Y plane without the detuning impedance.

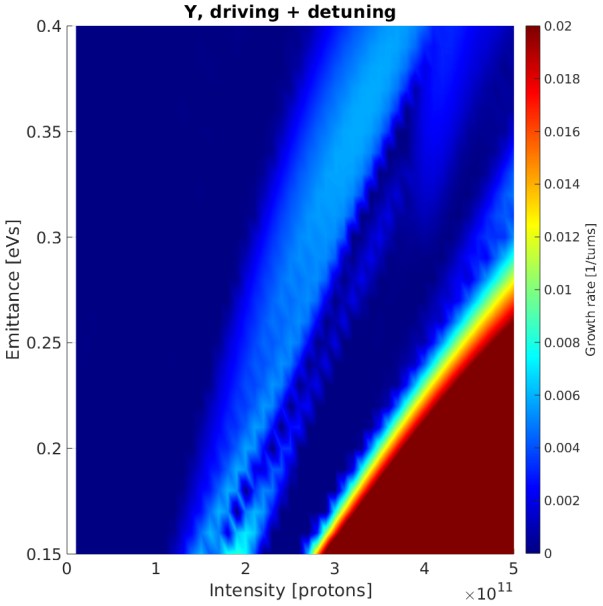

(d) Y plane with the detuning impedance.

Figure 11: Plot of emittance against intensity with the growth rate denoted in colour when considering linear synchrotron motion.

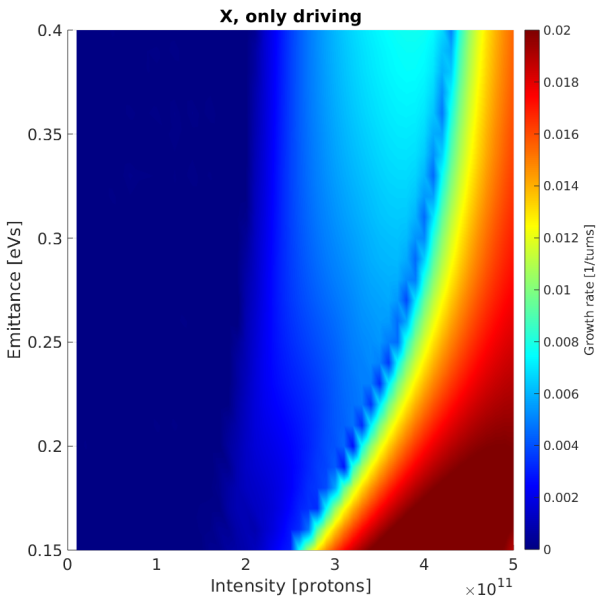

(a) X plane without the detuning impedance.

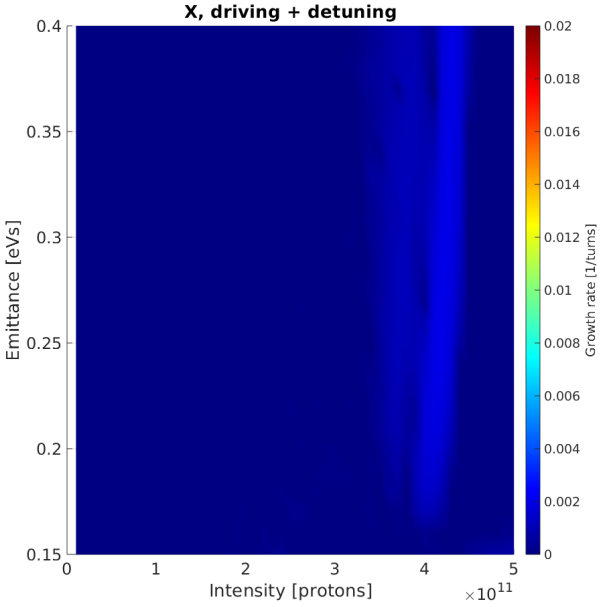

(b) X plane with the detuning impedance.

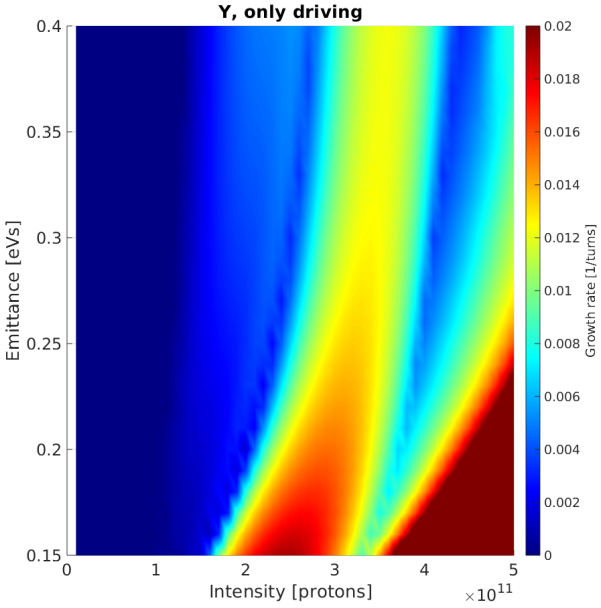

(c) Y plane without the detuning impedance.

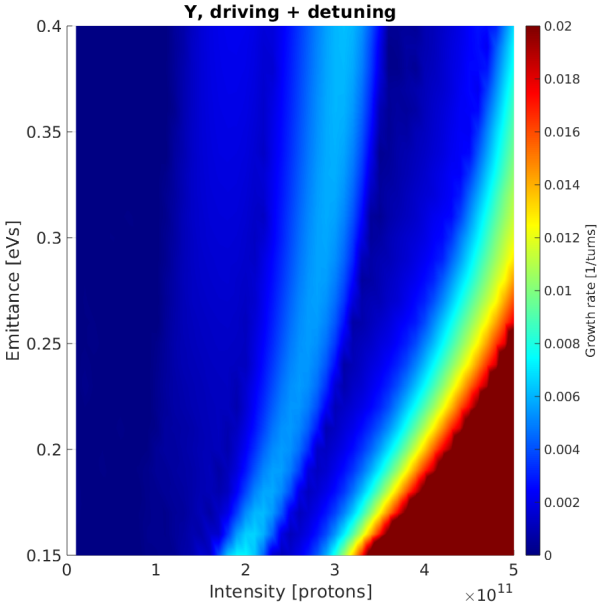

(d) Y plane with the detuning impedance.

Figure 12: Plot of emittance against intensity with the growth rate denoted in colour when considering non-linear synchrotron motion.

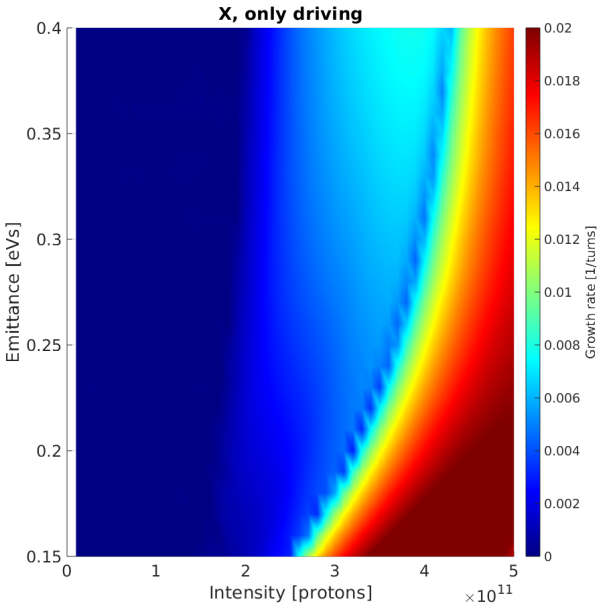

(a) X plane without the detuning impedance.

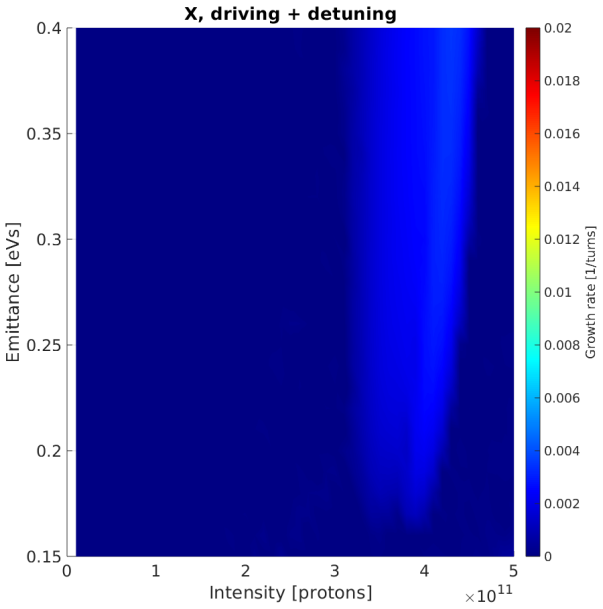

(b) X plane with the detuning impedance.

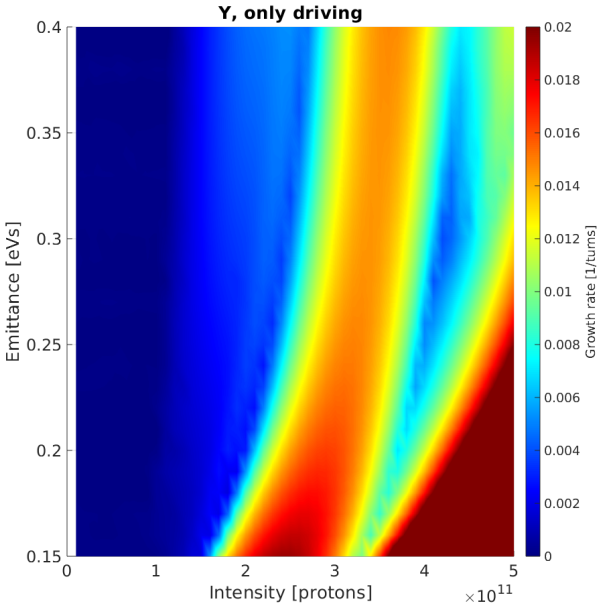

(c) Y plane without the detuning impedance.

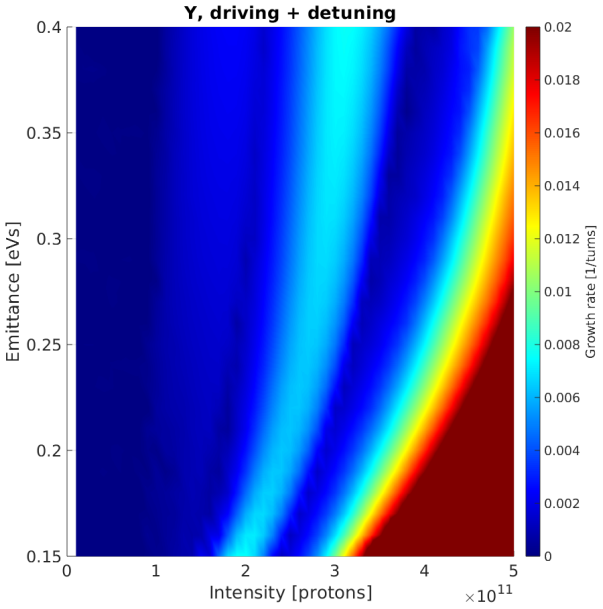

(d) Y plane with the detuning impedance.

Figure 13: Plot of emittance against intensity with the growth rate denoted in colour when considering non-linear synchrotron motion and second order chromaticities.

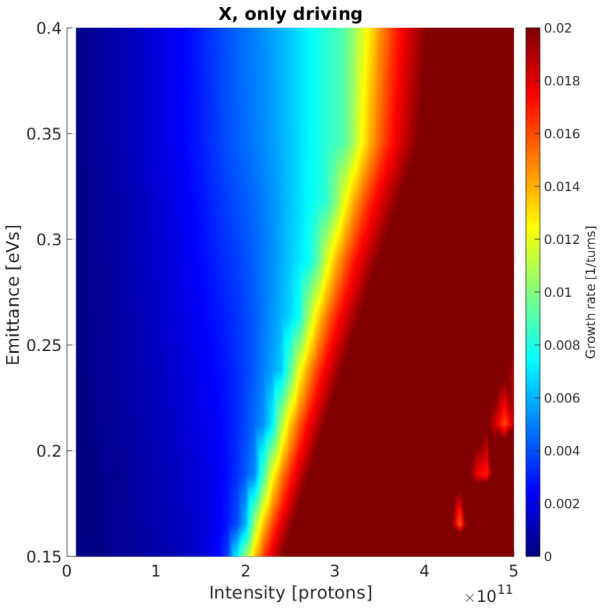

(a) X plane without the detuning impedance.

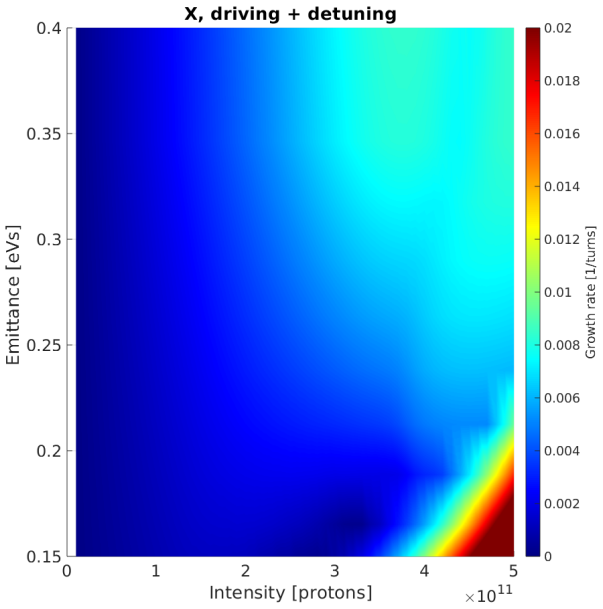

(b) X plane with the detuning impedance.

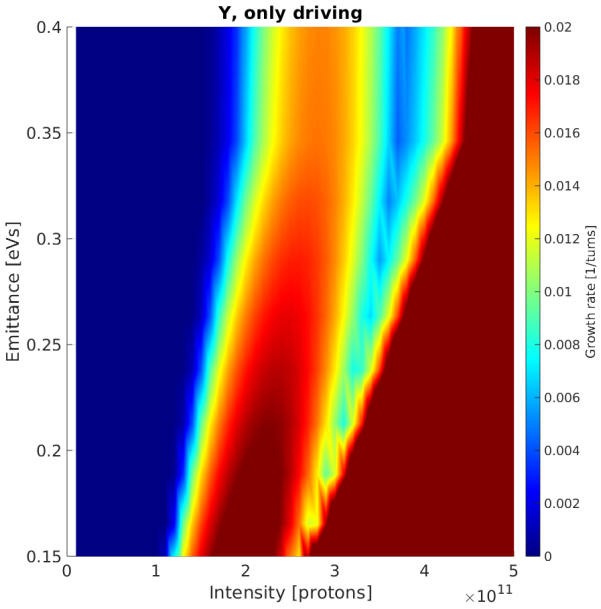

(c) Y plane without the detuning impedance.

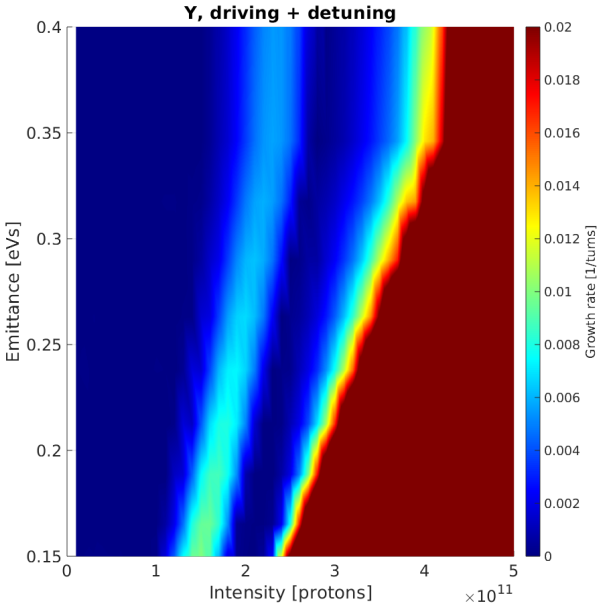

(d) Y plane with the detuning impedance.

Figure 14: Plot of emittance against intensity with the growth rate denoted in colour when considering non-linear synchrotron motion and up to third order chromaticities.

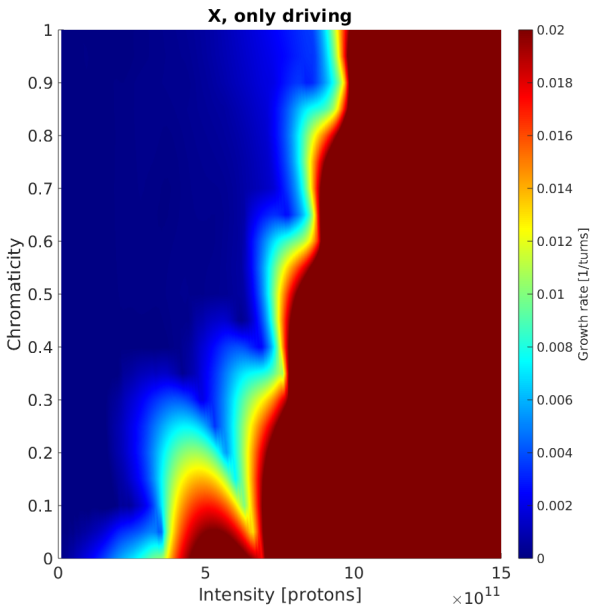

(a) X plane without the detuning impedance.

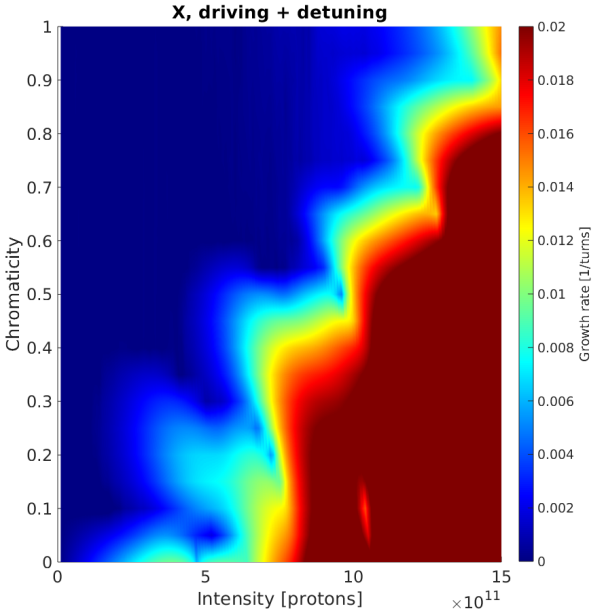

(b) X plane with the detuning impedance.

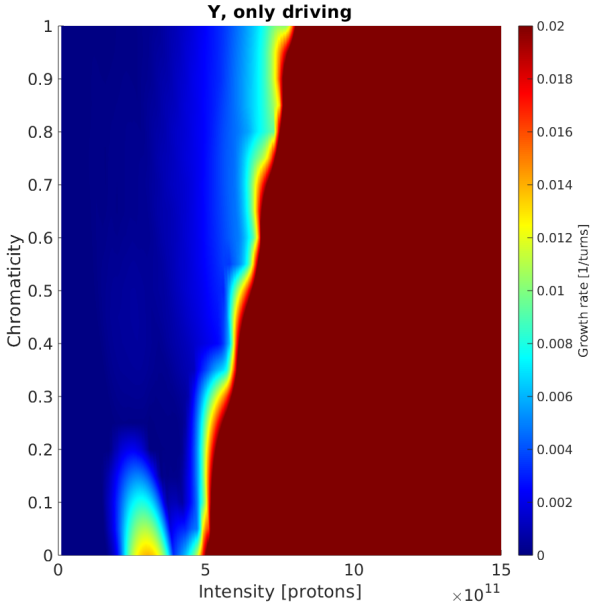

(c) Y plane without the detuning impedance.

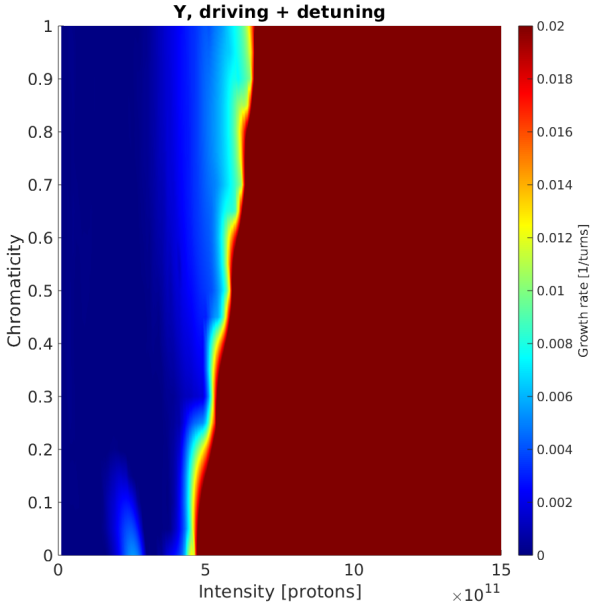

(d) Y plane with the detuning impedance.

Figure 15: Plot of chromaticity against intensity with the growth rate denoted in colour for Q-20 optics.

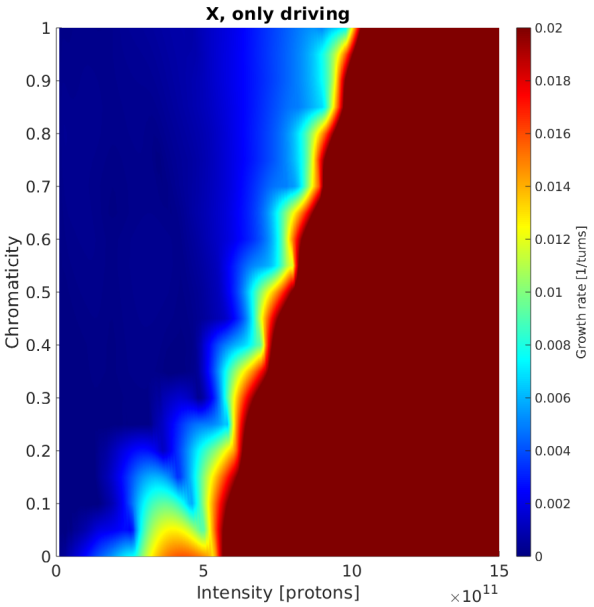

(a) X plane without the detuning impedance.

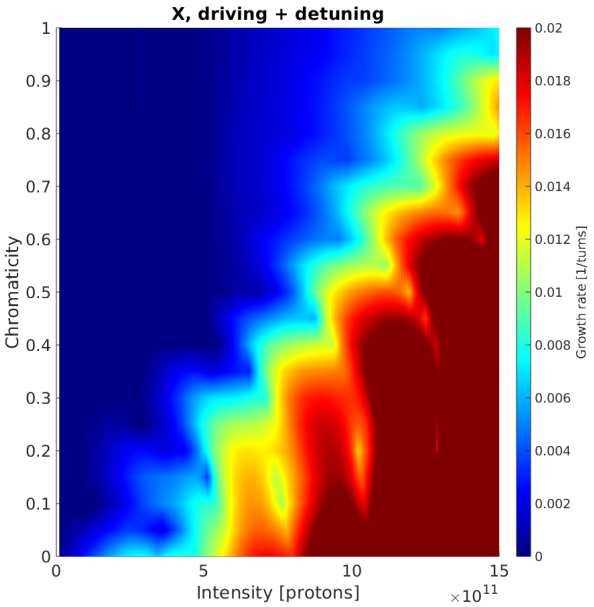

(b) X plane with the detuning impedance.

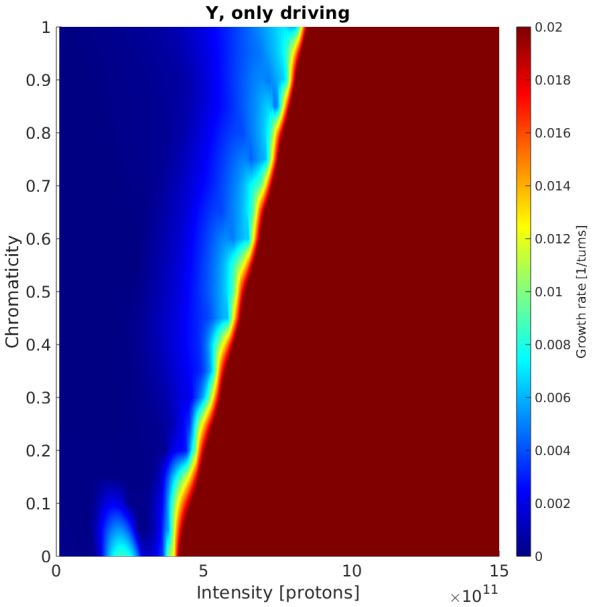

(c) Y plane without the detuning impedance.

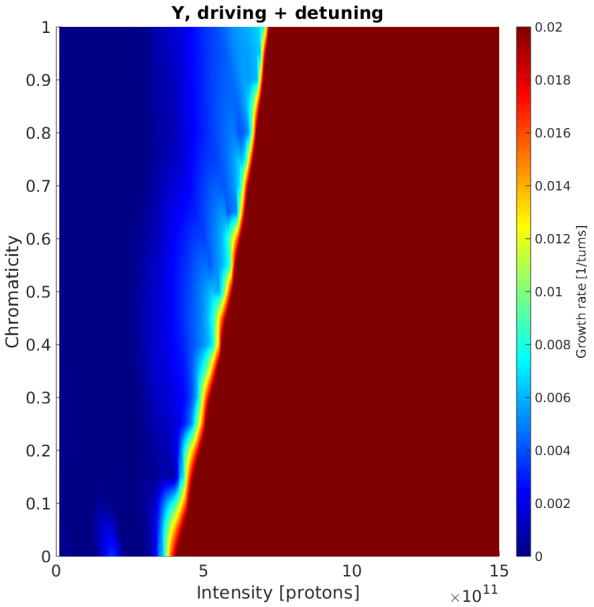

(d) Y plane with the detuning impedance.

Figure 16: Plot of chromaticity against intensity with the growth rate denoted in colour for Q-22 optics.

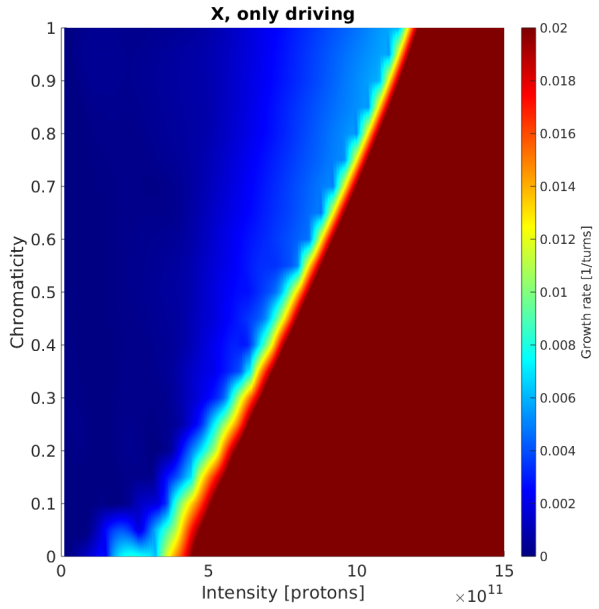

(a) X plane without the detuning impedance.

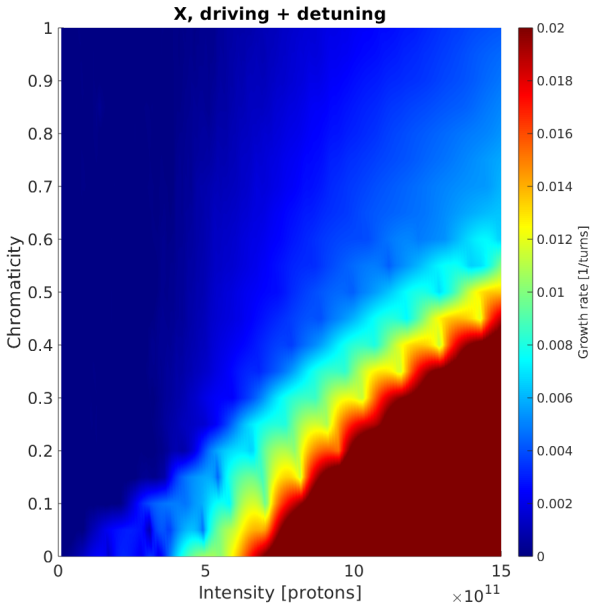

(b) X plane with the detuning impedance.

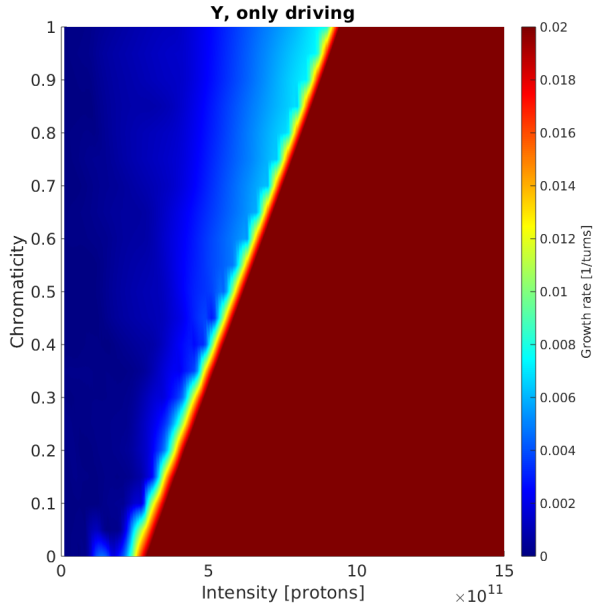

(c) Y plane without the detuning impedance.

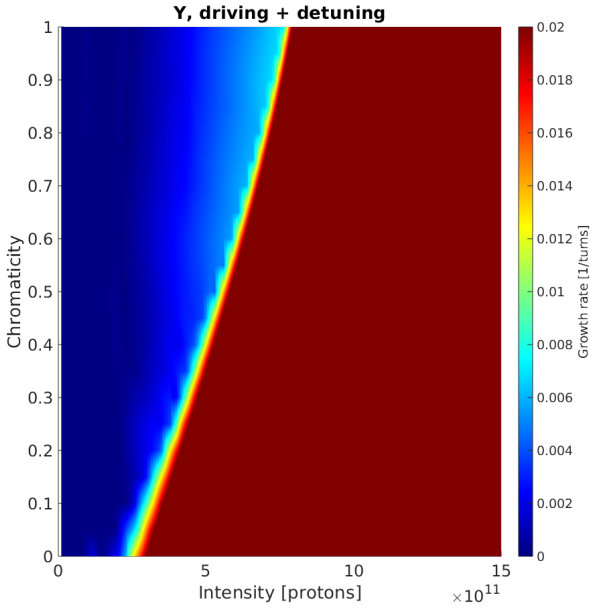

(d) Y plane with the detuning impedance.

Figure 17: Plot of chromaticity against intensity with the growth rate denoted in colour for Q-26 optics.

6 Analytical Model for Multi-Bunch Beam

This section describes an analytical model developed for rigid multi-bunch beam. Let M be the 2x2 one-turn map in the horizontal plane which is assumed to be linear and uncoupled. Then,

$$\begin{pmatrix} x \\ x' \end{pmatrix}_j = M * \begin{pmatrix} x \\ x' \end{pmatrix}_{j-1} \tag{1}$$

where $j \equiv$ turn number.

Throughout the analysis, only rigid bunches with one particle per bunch are considered and the transverse planes are assumed to be decoupled. If we consider no longitudinal motion, the longitudinal coordinates will be fixed. In that case we can assume $z_0 = 0$ without loss of generality. If we consider the positive Z axis in the direction opposite to direction of beam propagation, the Z coordinates of the bunches will be positive. The wakes produce only a kick and affect the momentum. If $\Delta x'_i$ denotes the wake kick due to the impedance in x for bunch i, the equation for the kick from [10] can be written as

$$\Delta x'_i = C \sum_{z_k < z_i} W_x(z_i - z_k, x_k, x_i) \tag{2}$$

for the conditions described, where $C = \frac{e^2}{E_0 \beta^2 \gamma}$ with $\beta = \sqrt{1 - \gamma^{-2}}$, E_0 being the rest mass of the elementary particles and e the elementary charge. The wake field W_x is given by

$$W_x(z, x_k, x_i) = W_x^{dip}(z) x_k + W_x^{quad}(z) x_i \tag{3}$$

The wakes are assumed to be single turn, i.e particles from previous turns do not create any wakes, and ultra-relativistic which gives $W(z = 0) = 0$. Substituting for the wake function gives,

$$\Delta x'_i = C \sum_{z_k < z_i} \left\{ W_x^{dip}(z_i - z_k) x_k + W_x^{quad}(z_i - z_k) x_i \right\} \tag{4}$$

Initially, 2 bunches are considered. The leading bunch can be denoted by the subscript 0 and the trailing bunch by the subscript 1. The wake kick on the trailing particle can then be written as,

$$\Delta x'_{1_j} = C \{ W_x^{dip}(z_1) x_{0_j} + W_x^{quad}(z_1) x_{1_j} \} \tag{5}$$

where the subscript j denotes the turn number. It should be noted that the wake kick depends on the coordinates of the same turn. Because of the absence of multi-turn effect, there is no kick felt by the leading particle. The wake kick is felt once during the turn and causes a change in the momentum. Hence the wake kick should be added to the x' term in equation (1). The one-turn equation for turn 1 including the wake kick can be written as,

$$\begin{aligned} \begin{pmatrix} x_1 \\ x'_1 \end{pmatrix}_1 &= M * \begin{pmatrix} x_1 \\ x'_1 \end{pmatrix}_0 + \begin{pmatrix} 0 \\ \Delta x'_1 \end{pmatrix} \\ &= M * \begin{pmatrix} x_1 \\ x'_1 \end{pmatrix}_0 + \begin{pmatrix} 0 \\ C\{W_x^{dip}(z_1) x_{0_1} + W_x^{quad}(z_1) x_{1_1}\} \end{pmatrix} \\ &= M * \begin{pmatrix} x_1 \\ x'_1 \end{pmatrix}_0 + \begin{pmatrix} 0 & 0 \\ C W_x^{dip}(z_1) & C W_x^{quad}(z_1) \end{pmatrix} \begin{pmatrix} x_{0_1} \\ x_{1_1} \end{pmatrix} \end{aligned} \tag{6}$$

For convenience, consider an intermediate coordinate vector for turn 1 resulting from the transfer matrix. Then,

$$\begin{pmatrix} x_1 \\ x_1' \end{pmatrix}_{1,int} = M * \begin{pmatrix} x_1 \\ x_1' \end{pmatrix}_0 \tag{7}$$

The final coordinate vector for turn 1 can be obtained by applying the wake kick to the intermediate coordinate vector for turn 1.

$$\begin{pmatrix} x_1 \\ x_1' \end{pmatrix}_1 = \begin{pmatrix} x_1 \\ x_1' \end{pmatrix}_{1,int} + \begin{pmatrix} 0 \\ CW_x^{dip}(z_1)x_{0_{1,int}} + CW_x^{quad}(z_1)x_{1_{1,int}} \end{pmatrix} \tag{8}$$

It should be noted that equation (8) holds because the wake produces only a kick and does not affect the bunch position. As the wake kick for bunch 0 is $\Delta x_0' = 0$, the equation for particle 0 can be written as,

$$\begin{pmatrix} x_0 \\ x_0' \end{pmatrix}_1 = M * \begin{pmatrix} x_0 \\ x_0' \end{pmatrix}_0 \tag{9}$$

This can be generalised to include both bunches to give the equation,

$$\begin{pmatrix} x_0 \\ x_0' \\ x_1 \\ x_1' \end{pmatrix}_{1,int} = T * \begin{pmatrix} x_0 \\ x_0' \\ x_1 \\ x_1' \end{pmatrix}_0 \tag{10}$$

where $T \equiv$ transfer matrix $= \begin{pmatrix} M & O \\ O & M \end{pmatrix}$, where M is the 2×2 one-turn map and O is a 2x2 null matrix. Using equation (10), the final turn 1 coordinates are given by,

$$\begin{aligned} \begin{pmatrix} x_0 \\ x_0' \\ x_1 \\ x_1' \end{pmatrix}_1 &= \begin{pmatrix} x_0 \\ x_0' \\ x_1 \\ x_1' \end{pmatrix}_{1,int} + \begin{pmatrix} 0 & 0 & 0 & 0 \\ 0 & 0 & 0 & 0 \\ 0 & 0 & 0 & 0 \\ CW_x^{dip}(z_1) & 0 & CW_x^{quad}(z_1) & 0 \end{pmatrix} \begin{pmatrix} x_0 \\ x_0' \\ x_1 \\ x_1' \end{pmatrix}_{1,int} \\ &= \left\{ I + \begin{pmatrix} 0 & 0 & 0 & 0 \\ 0 & 0 & 0 & 0 \\ 0 & 0 & 0 & 0 \\ CW_x^{dip}(z_1) & 0 & CW_x^{quad}(z_1) & 0 \end{pmatrix} \right\} \begin{pmatrix} x_0 \\ x_0' \\ x_1 \\ x_1' \end{pmatrix}_{1,int} \\ &= \left\{ I + \begin{pmatrix} 0 & 0 & 0 & 0 \\ 0 & 0 & 0 & 0 \\ 0 & 0 & 0 & 0 \\ CW_x^{dip}(z_1) & 0 & CW_x^{quad}(z_1) & 0 \end{pmatrix} \right\} \{T\} \begin{pmatrix} x_0 \\ x_0' \\ x_1 \\ x_1' \end{pmatrix}_0 \end{aligned} \tag{11}$$

with I being an identity matrix of appropriate dimensions.

The same model can be extended to include 3 bunches. The wake kick for bunch 2 in turn j can be obtained from equation (4).

$$\Delta x_{2_j}' = C\{W_x^{dip}(z_2)x_{0_j} + W_x^{dip}(z_2 - z_1)x_{1_j} + \left[W_x^{quad}(z_2) + W_x^{quad}(z_2 - z_1)\right] x_{2_j}\} \tag{12}$$

$$\begin{aligned}\begin{pmatrix} x_0 \\ x_0' \\ x_1 \\ x_1' \\ x_2 \\ x_2' \end{pmatrix}_1 &= \{I+W\}\{T\} \begin{pmatrix} x_0 \\ x_0' \\ x_1 \\ x_1' \\ x_2 \\ x_2' \end{pmatrix}_0 \\ &= \{T+WT\} \begin{pmatrix} x_0 \\ x_0' \\ x_1 \\ x_1' \\ x_2 \\ x_2' \end{pmatrix}_0 \end{aligned} \tag{13}$$

$$W = \begin{pmatrix} 0 & 0 & 0 & 0 & 0 & 0 \\ 0 & 0 & 0 & 0 & 0 & 0 \\ 0 & 0 & 0 & 0 & 0 & 0 \\ CW_x^{dip}(z_1) & 0 & CW_x^{quad}(z_1) & 0 & 0 & 0 \\ 0 & 0 & 0 & 0 & 0 & 0 \\ CW_x^{dip}(z_2) & 0 & CW_x^{dip}(z_2-z_1) & 0 & CW_x^{quad}(z_2)+CW_x^{quad}(z_2-z_1) & 0 \end{pmatrix}$$

is the wake matrix, and $T = \begin{pmatrix} M & O & O \\ O & M & O \\ O & O & M \end{pmatrix}$ is similar to that defined when considering two bunches.

Extending to n bunches but still maintaining the same assumptions, the matrices can be defined as,

$$T_{n\times n} = \begin{pmatrix} M & O & \dots & O \\ O & M & \dots & O \\ \vdots & \vdots & \ddots & \vdots \\ O & O & \dots & M \end{pmatrix} \tag{14}$$

where every element is a 2x2 matrix, and

$$W_{2n\times 2n} = \begin{pmatrix} 0 & 0 & \dots & 0 & \dots & 0 \\ 0 & 0 & \dots & 0 & \dots & 0 \\ 0 & 0 & \dots & 0 & \dots & 0 \\ CW_x^{dip}(z_1) & 0 & CW_x^{quad}(z_1) & 0 & \dots & 0 \\ 0 & 0 & \vdots & \ddots & \dots & 0 \\ \vdots & & & & & \vdots \\ CW_x^{dip}(z_n) & 0 & CW_x^{dip}(z_n-z_1) & \dots & C\sum_{z_k<z_n} W_x^{quad}(z_n-z_k) & 0 \end{pmatrix} \tag{15}$$

The 2x2 transfer matrix M is given by

$$M = \begin{pmatrix} \cos\mu + \alpha\sin\mu & \beta\sin\mu \\ -\gamma\sin\mu & \cos\mu - \alpha\sin\mu \end{pmatrix} \tag{16}$$

$$\det M = 1 \Rightarrow \beta\gamma - \alpha^2 = 1 \tag{17}$$

Assuming a smooth approximation, $\alpha = 0$. The β is given by,

$$\beta = \frac{R}{Q} \tag{18}$$

where $R \equiv$ average machine radius and $Q \equiv$ the tune.
For the SPS with $R = \frac{6911}{2\pi}$ and assuming Q-20 optics, $Q = 20.13$ for the X axis, $\beta = 54.64$.

$$\alpha = 0 \Rightarrow \gamma = \frac{1}{\beta} = 0.0183$$

The parameter $\mu \equiv$ phase advance of each turn and is given by,

$$\mu = 2\pi Q \tag{19}$$

which for the SPS computes to $\mu = 126.48$. Substituting the values we get,

$$M = \begin{pmatrix} \cos 126.48 & 54.55 \sin 126.48 \\ -0.0183 \sin 126.48 & \cos 126.48 \end{pmatrix} = \begin{pmatrix} 0.6845 & 39.8314 \\ -0.0133 & 0.6845 \end{pmatrix} \tag{20}$$

α_X	0	α_Y	0
β_X	54.64	β_Y	54.50
γ_X	0.0183	γ_Y	0.0183
μ_X	126.48	μ_Y	126.79
Q_X	20.13	Q_Y	20.18

Table 1: Parameter values for the SPS with Q20 optics

Let $v_1, v_2, ..., v_{2n}$ be the eigenvectors and $\lambda_1, \lambda_2, ..., \lambda_{2n}$ be the corresponding eigenvalues of $\{(I + W)T\}$ where n is the number of rigid bunches. Assuming the matrix can be diagonalised, any vector can be expressed as a linear combination of the eigenvectors. Hence,

$$\begin{pmatrix} x_0 \\ x'_0 \\ \vdots \\ x_{n-1} \\ x'_{n-1} \end{pmatrix}_0 = Av_1 + Bv_2 + ... + Nv_{2n} \tag{21}$$

for vector of positions and momenta corresponding to turn 0 and

$$\{(I + W)T\}^m \begin{pmatrix} x_0 \\ x'_0 \\ \vdots \\ x_{n-1} \\ x'_{n-1} \end{pmatrix}_0 = A\lambda_1^m v_1 + B\lambda_2^m v_2 + ... + N\lambda_{2n}^m v_{2n} \tag{22}$$

for that of turn m. As $\{(I+W)T\} \in \mathbb{R}$, the eigenvalues are complex conjugates. Hence the pairs of eigenvalues for mode i can be represented by $\lambda_{i_{1,2}} = r_i e^{\pm j\mu_i}$. From the properties of eigenvalues and from our representation,

$$\begin{aligned} tr\,\{(I+W)T\} &= \sum_{i=1}^{n} \lambda_{i_1} + \lambda_{i_2} \\ &= 2\sum_{i=1}^{n} r_i \cos\mu_i \end{aligned} \tag{23}$$

and

$$\begin{aligned} det\,\{(I+W)T\} &= \prod_{i=1}^{n} \lambda_{i_1}\lambda_{i_2} \\ &= \prod_{i=1}^{n} r_i^2 \end{aligned} \tag{24}$$

It should be noted that in absence of wakes, the determinant is 1 and $r_i = 1$ for all i. For stability, $\lambda_{i_{1,2}}^m$ must not grow with m. Hence we get the condition $|r_i| \leq 1$ from equation (22). Now if we consider the mode $i = 1$, with the eigenvalues $\lambda_{1_1} = r_1 e^{j\mu_1}$ and $\lambda_{1_2} = r_1 e^{-j\mu_1}$ we get,

$$\begin{aligned} \lambda_{1_1} + \lambda_{1_2} &= 2r_1\cos\mu_1 \\ &= 2\sqrt{\lambda_{1_1}\lambda_{1_2}}\cos\mu_1 \\ \Rightarrow \mu_1 &= \arccos\frac{\lambda_{1_1}+\lambda_{1_2}}{2\sqrt{\lambda_{1_1}\lambda_{1_2}}} \end{aligned} \tag{25}$$

Equation (25) is useful for calculating the tune of each mode from the eigenvalues. A plot of the tunes thus obtained can be seen in Fig. 18. The obtained tunes have been sorted according to the imaginary part of the eigenvalues. The plots make it clear that in the presence of both driving and detuning wakes, it is the detuning wake that dominates the tune shift.

To include the effect of a damper, an additional term related to the damper gain needs to be added to the matrix. An ideal damper can be seen as reducing the bunch positions by a finite value by applying a negative kick without affecting the bunch momentum. As the term due to the damper is independent of the wakes, the damper term can be added to the transfer matrix. If we consider a single bunch with the coordinates $\begin{pmatrix} x_0 \\ x_0' \end{pmatrix}$ with no wakes, then the coordinates for turn j in terms of turn $(j-1)$ are given by

$$\begin{pmatrix} x_0 \\ x_0' \end{pmatrix}_j = M * \begin{pmatrix} x_0 \\ x_0' \end{pmatrix}_{j-1} \tag{26}$$

where $M \equiv$ transfer. Let the transfer matrix be given by

$$M = \begin{pmatrix} a & b \\ c & d \end{pmatrix} \tag{27}$$

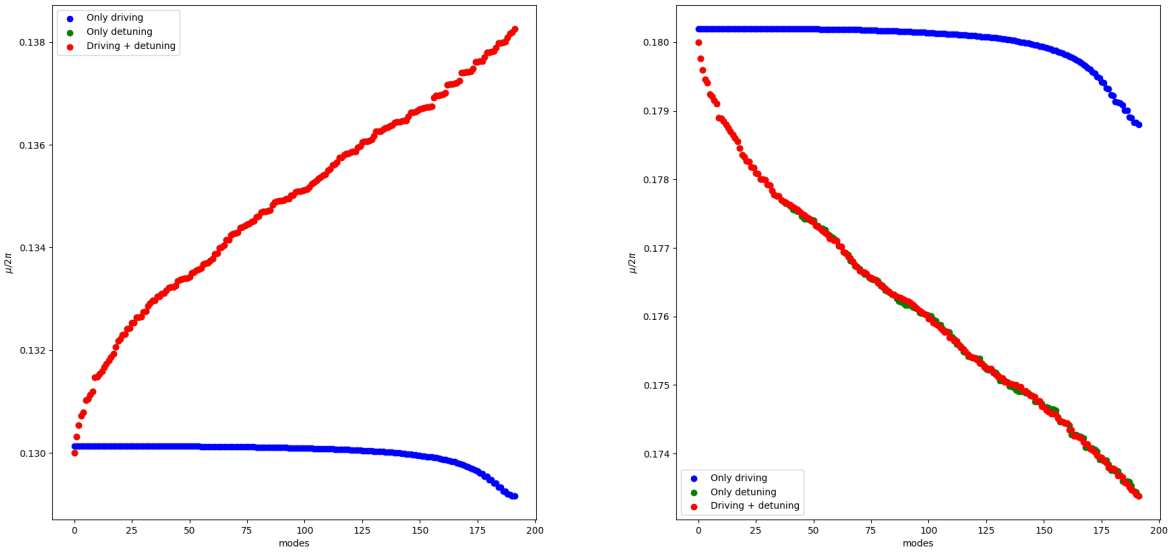

(a) X tune. (b) Y tune.

Figure 18: Plot of tunes obtained from equation (25) against modes. It should be noted that the tunes obtained from the only detuning (in red) and the case of driving and detuning (in green) overlap and hence only the red curve is visible.

We can write the bunch coordinates as,

$$\begin{aligned} x_{0_j} &= a x_{0_{j-1}} + b x'_{0_{j-1}} \\ x'_{0_j} &= c x_{0_{j-1}} + d x'_{0_{j-1}} \end{aligned} \tag{28}$$

As the damper acts on and affects only the bunch position and not the momentum, after introduction of the damper, the bunch position is given by,

$$\begin{aligned} x_{0_j} &= a x_{0_{j-1}} + b x'_{0_{j-1}} - g x_{0_{j-1}} \\ &= (a-g) x_{0_{j-1}} + b x'_{0_{j-1}} \end{aligned} \tag{29}$$

where $g \equiv$ damper gain. The new transfer matrix is then given by,

$$M_{damper} = \begin{pmatrix} a-g & b \\ c & d \end{pmatrix} \tag{30}$$

Turn by turn tracking was carried out with this analytical model using python for an intensity of 1×10^{11} protons/bunch over 8192 turns. The bunch by bunch tune shift was evaluated using HarPy. The code used for this is available in Ref. [15]. The obtained tune shifts without considering a damper are seen in Fig. 19 and with a damper gain (defined according to the equation 30) of 0.01 in Fig. 20.

From Fig. 20a, we can see that introducing a damper results in a flat tune with bunches while without a damper jumps in the tune are observed. In an ideal case with all bunches

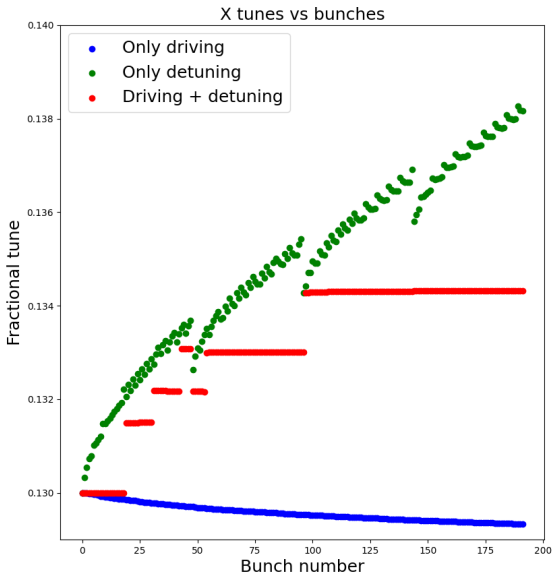

(a) X tune.

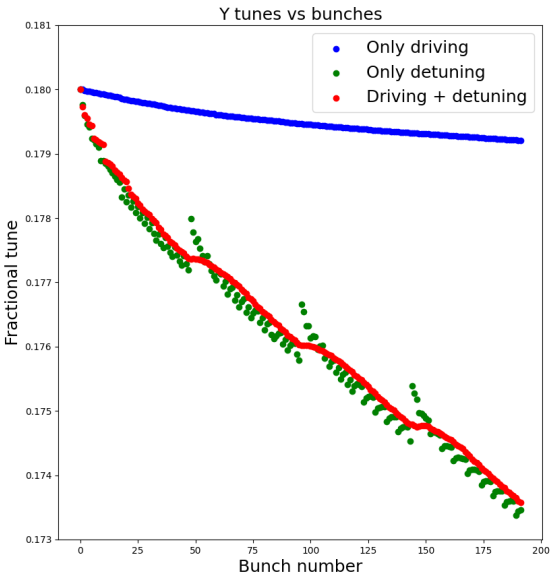

(b) Y tune.

Figure 19: Plot of bunch by bunch tunes without damper.

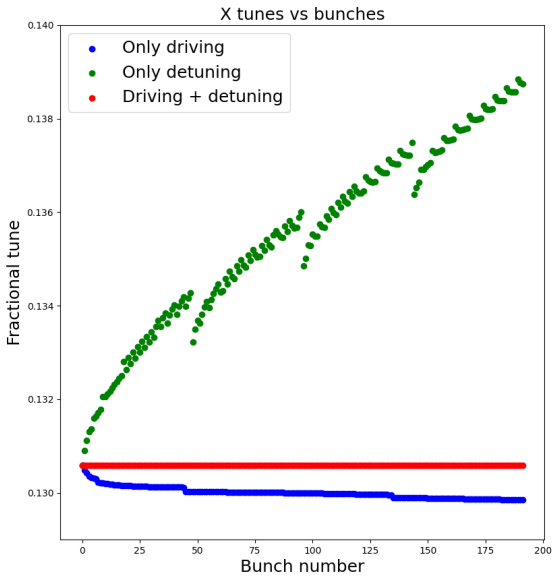

(a) X tune.

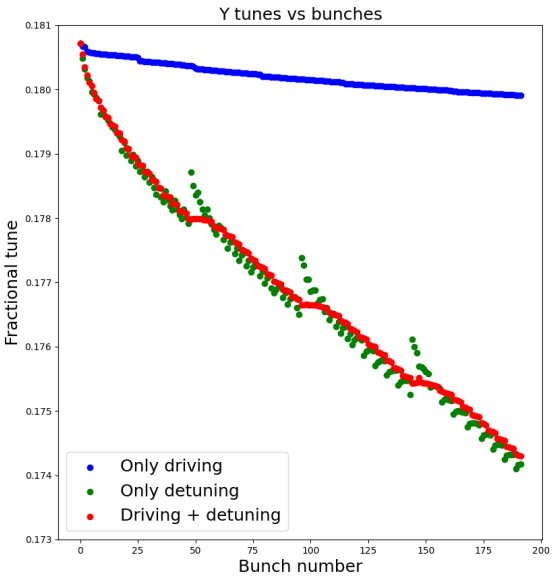

(b) Y tune.

Figure 20: Plot of bunch by bunch tunes with a damper gain of 0.01.

stable, in the horizontal plane, the driving and detuning wakes are equal and opposite and are expected to cancel each other's tune shifts giving a flat tune plot. However, this is not observed in Fig. 19a. A closer look at the horizontal plane bunch positions revealed that in absence of a damper some of the bunches were unstable and oscillating with a different amplitude, while some were still stable. As a result, the bunches behind the bunches with a larger amplitude experience a larger contribution to the kick as compared to the other bunches due to its larger offset from the symmetry axis (from equation (4)). Such an effect perturbs the oscillation causing the change in the tunes seen in Fig. 19a.

In the condition explained above without a damper, the behaviour of the tune shifts versus the number of turns analysed is also worth investigating. For a low intensity, it will take a larger number of turns for the instability to be appreciable and the opposite will be true for a higher intensity. Figure 21 shows a plot of the maximum tune excursion against the number of turns considered in the X and Y planes for two different intensities on a logarithmic X scale. For the case with both driving and detuning wakes, an increase in the tune is seen at a lower number of turns for a higher intensity (see Fig. 21a) since a certain oscillation amplitude will be reached after a lower number of turns. No such increase is seen in the vertical plane since the instability in the vertical plane is expected to be significantly lower. Fig. 21 also shows that the tune shift with only the driving impedance tends to zero when increasing the number of turns analysed while the tune shift with only the detuning impedance converges very quickly.

To verify the converse, the maximum tune excursions for different number of turns were plotted against the intensity and can be seen in Figs. 22-24. In Fig. 24a it can be seen that even at higher intensities, for a lower number of turns, the amplitude of the instability is not appreciable enough to cause an increase in the tune. But for a higher number of turns, there is enough time for the instability to become appreciable and in such situations, the intensity effect is clearly seen. A threshold phenomenon is observed where there is a sudden rise in the tune shifts and the threshold intensity reduces with higher number of turns as can be seen for 4096 and 8192 turns from Fig. 24a. No such effect is seen in the vertical plane since the instability growth rate is not high enough to generate a perturbation with tune in the explored intensity range over the number of turns analysed.

All the above analysis is has been performed considering single-turn wakes as the equation (4) holds only for single-turn wakes. Even though this is a reasonable approximation for the SPS wake, in practice, wakes are often multi-turn as they decay over several turns and not just a single turn. When considering wake memory, all the bunches need to be considered over n_{wake} turns. It is convenient to develop a model by separating the dipolar and quadrupolar wake kicks. The new expressions for the kick experienced by bunch i in turn j are given by,

$$\begin{aligned} \Delta^{dip}x_{i_j} &= C \sum_{k=0}^{n_{wake}-1} \sum_{s=0}^{n-1} W_x^{dip}(kS + (z_i - z_s))x_{s_{j-k}} \\ \Delta^{quad}x_{i_j} &= C \sum_{k=0}^{n_{wake}-1} \sum_{s=0}^{n-1} W_x^{quad}(kS + (z_i - z_s))x_{i_j} \end{aligned} \tag{31}$$

where $\Delta^{dip}x_{i_j}$ is the dipolar kick, $\Delta^{quad}x_{i_j}$ is the quadrupolar kick and $S \equiv$ circumference of the machine. It should be noted that because of the multi-turn effect, a particular bunch i

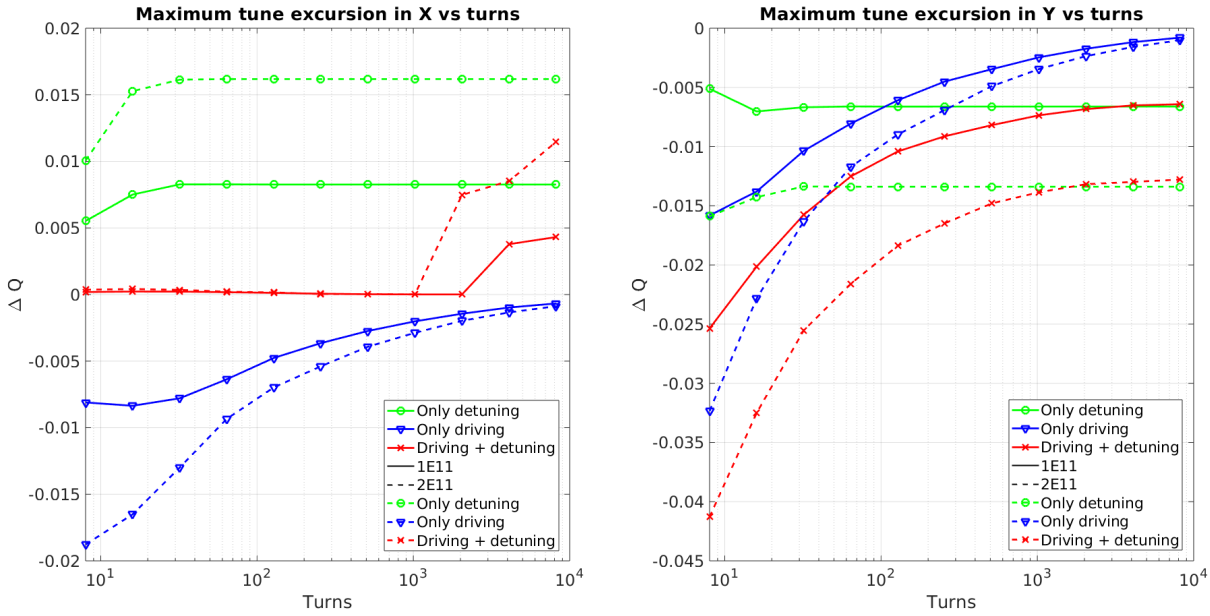

(a) ΔQ_x (b) ΔQ_y

Figure 21: Plot of the tune shift against the number of turns for different intensities.

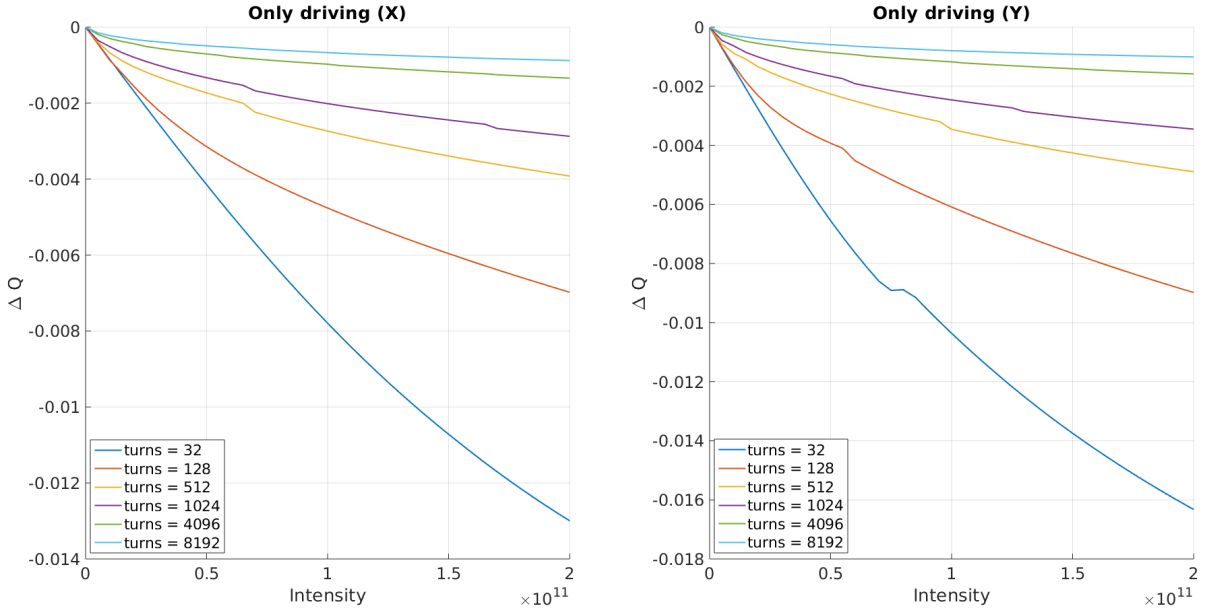

(a) ΔQ_x (b) ΔQ_y

Figure 22: Plot of the tune shift against intensity in the presence of only driving wakes for different number of turns.

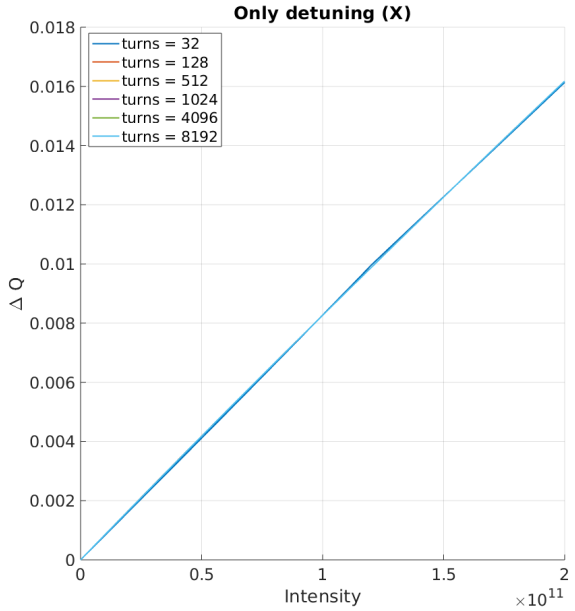

(a) ΔQ_x

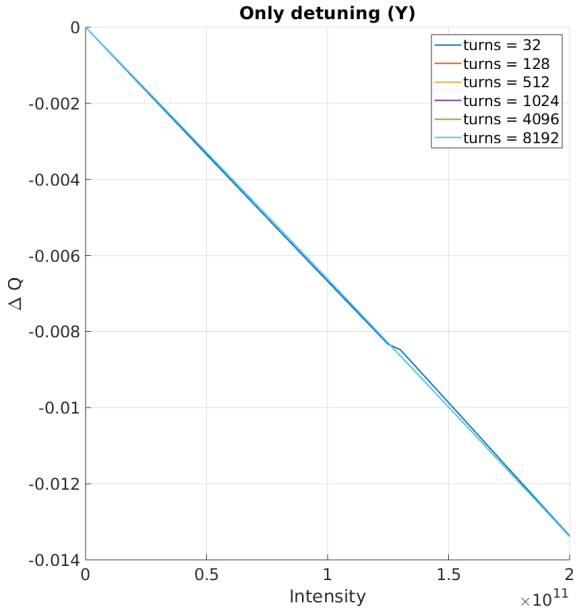

(b) ΔQ_y

Figure 23: Plot of the tune shift against intensity in the presence of only detuning wakes for different number of turns.

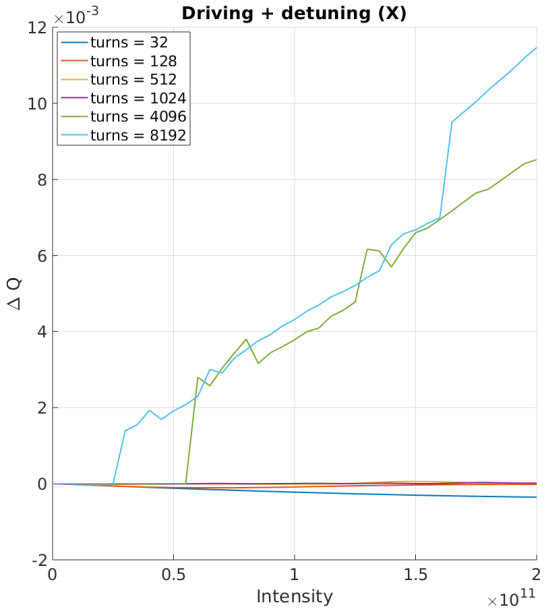

(a) ΔQ_x

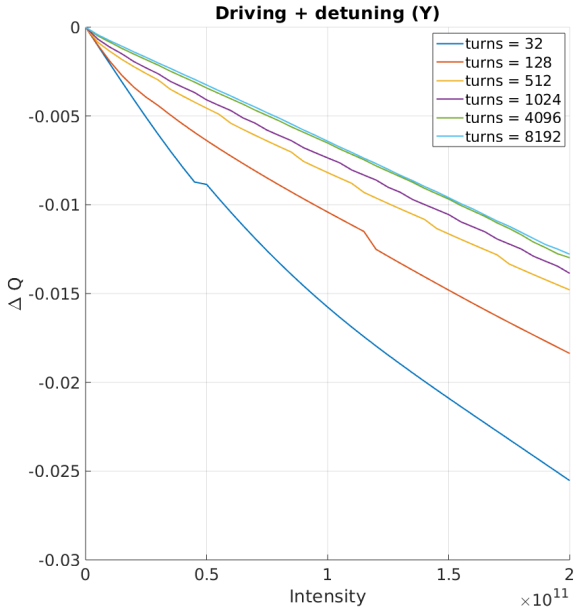

(b) ΔQ_y

Figure 24: Plot of the tune shift against intensity in the presence of both driving and detuning wakes for different number of turns.

will be affected by the wakes of all other bunches and not just the ones ahead of it. From equation (31), the wake matrix of equation (15) needs to be rewritten as a function of the turn number k. As the dipolar wake kick depends on previous turn coordinates too, while the quadrupolar wake kick depends only on the present turn, it is convenient to define two different matrices, $W^{dip}_{2n\times 2n}(k)$ for the dipolar wakes and $W^{quad}_{2n\times 2n}(k)$ for the quadrupolar wakes

$$\mathrm{W}^{dip}_{2n\times 2n}(k) = \begin{pmatrix} 0 & 0 & \dots & \dots & \dots & 0 \\ CW_x^{dip}(kS+0) & 0 & CW_x^{dip}(kS+(-z_1)) & \dots & CW_x^{dip}(kS+(-z_{n-1})) & 0 \\ 0 & 0 & \dots & \dots & \dots & 0 \\ CW_x^{dip}(kS+z_1) & 0 & CW_x^{dip}(kS+0) & \dots & CW_x^{dip}(kS+(z_1-z_{n-1}) & 0 \\ 0 & 0 & \vdots & \ddots & \dots & 0 \\ \vdots & & & & & \vdots \\ CW_x^{dip}(kS+z_{n-1}) & 0 & CW_x^{dip}(kS+(z_{n-1}-z_1)) & \dots & CW_x^{dip}(kS+0) & 0 \end{pmatrix} \tag{32}$$

$$\mathrm{W}^{quad}_{2n\times 2n}(k) = \begin{pmatrix} 0 & 0 & \dots & \dots & 0 \\ \sum_{s=0}^{n-1} W_x^{quad}(kS+(-z_s)) & 0 & \dots & \dots & 0 \\ 0 & 0 & \dots & \dots & 0 \\ 0 & 0 & \sum_{s=0}^{n-1} W_x^{quad}(kS+(z_1-z_s)) & \dots & 0 \\ 0 & 0 & \ddots & \dots & 0 \\ \vdots & & & & \vdots \\ 0 & 0 & 0 & \sum_{s=0}^{n-1} W_x^{quad}(kS+(z_{n-1}-z_s)) & 0 \end{pmatrix} \tag{33}$$

Let the vector of coordinates for turn j be defined by X_j where $X_j = \begin{pmatrix} x_0 \\ x_0' \\ \vdots \\ x_{n-1} \\ x_{n-1}' \end{pmatrix}_j$. The dipolar and quadrupolar kicks can then be written in matrix form as,

$$\Delta^{dip} X_j = \sum_{k=0}^{n_{wake}-1} W^{dip}_{2n\times 2n}(k) X_{j-k} \tag{34}$$

$$\Delta^{quad} X_j = \sum_{k=0}^{n_{wake}-1} W^{quad}_{2n\times 2n}(k) X_j \tag{35}$$

respectively. The intermediate coordinate vector defined similar to equation (7) after applying the transfer matrix is then given by,

$$X_{j,int} = T X_{j-1} \tag{36}$$

The final coordinates for the j^{th} turn are obtained by applying the kick,

$$\begin{aligned} X_j &= X_{j,int} + \sum_{k=0}^{n_{wake}-1} W^{quad}_{2n\times 2n}(k) X_{j,int} + W^{dip}_{2n\times 2n}(0) X_{j,int} + \sum_{k=1}^{n_{wake}-1} W^{dip}_{2n\times 2n}(k) X_{j-k} \\ &= \left\{ I + \sum_{k=0}^{n_{wake}-1} W^{quad}_{2n\times 2n}(k) + W^{dip}_{2n\times 2n}(0) \right\} T X_{j-1} + \sum_{k=1}^{n_{wake}-1} W^{dip}_{2n\times 2n}(k) X_{j-k} \end{aligned} \tag{37}$$

Of course, the equation (37) is valid only because the quadrupolar kick always depends on the instantaneous position of the bunch and not on the positions in previous turns. Let

$Y_{j-1} = \begin{pmatrix} X_{j-1} \\ X_{j-2} \\ \vdots \\ X_{j-(n_{wake}-1)} \end{pmatrix}$ be defined as the vector of the coordinates of all previous $n_{wake} - 1$ turns. The equation (37) can then be written in a matrix form as,

$$Y_j = \{A + B\} Y_{j-1} \tag{38}$$

where

$$A = \begin{pmatrix} \left\{ I + \sum_{k=0}^{n_{wake}-1} W^{quad}_{2n\times 2n}(k) + W^{dip}_{2n\times 2n}(0) \right\} T & O & \dots & O & O \\ I & O & \dots & O & O \\ O & I & \dots & O & O \\ \vdots & \vdots & \ddots & \vdots & \vdots \\ O & O & \dots & I & O \end{pmatrix}$$

and

$$B = \begin{pmatrix} W^{dip}_{2n\times 2n}(1) & W^{dip}_{2n\times 2n}(2) & \dots & W^{dip}_{2n\times 2n}(n_{wake}-1) \\ O & O & \dots & O \\ \vdots & \vdots & \ddots & \vdots \\ O & O & \dots & O \end{pmatrix}$$

with $I \equiv 2n \times 2n$ identity matrix and $O \equiv 2n \times 2n$ null matrix.

7 Conclusion

An extensive study of the effects of the detuning impedance was carried out by considering different factors. Particle tracking simulations of Sec. 3 with the two particle model confirmed the predictions of [16], where the detuning impedance is expected to always stabilise for zero chromaticity in the TMCI regime. With a large number of macroparticles, the effect of the detuning impedance seems to depend on the second harmonic voltage. From this, it can be inferred that the actual distribution of the particles plays an important role in how the impedance affects the beam. For linear synchrotron motion, the detuning impedance always stabilises while for non-linear synchrotron motion with a single harmonic RF voltage, mode 1 of intra bunch motion is destabilised. As the second harmonic voltage is increased as a percentage of the first, the destabilising effect is reduced more and more till a stabilising effect is observed beyond which the detuning impedance always stabilises. For negative chromaticity, it can be inferred that the growth rate can be estimated from only the driving impedance.

An effect is seen on the TMCI threshold as well. For a realistic SPS impedance model, the effect on the threshold is seen to be highly favourable. It has been observed that at higher longitudinal beam emittances, it is the higher order chromaticities that prove to be limiting on the threshold as compared to the detuning impedance since these higher order effects reduce the threshold. In absence of these higher order effects, there is a significant increase in the threshold due to the detuning impedance. At high positive chromaticities too, it is seen that the detuning impedance does not play a critical role in the vertical plane.

In the horizontal plane, however, there is a significant increase in the threshold at higher positive chromaticities in presence of the detuning impedance. A phenomenon of particular note was observed with respect to the optics. An increasing value of the threshold is observed with optics in the order Q-26, Q-22 and Q-20 while for higher positive chromaticities, this order is reversed due to the higher chromatic frequency shift for the same chromaticity unit in different optics.

The Vlasov solver based EDELPHI code is found to give results in good agreement with the ones obtained from PyHEADTAIL. This exercise has served as a means of verifying the results obtained from particle tracking and also increase confidence in the EDELPHI solver. From this solver, the effect of the detuning impedance on the tune shifts and coupling of transverse modes could be studied in a more detailed manner than possible with particle tracking. Such a detailed tune analysis allowed finding exactly which modes couple to lead to the TMCI.

An analytical model for the calculation of the bunch by bunch tune shift with both the driving and the detuning impedances, and a damper has also been developed. The model has been tested with the SPS wall wake to disentangle the effect of the driving and the detuning impedance. It has also been used to study the behaviour of the tune shift over the number of turns analysed.

Acknowledgement

G. Iadarola, D. Amorim, B. Salvant, X. Buffat, H. Bartosik, E. Métral

References

[1] C. Zannini, "Electromagnetic Simulation of CERN accelerator Components and Experimental Applications," Mar 2013. Presented 15 Apr 2013.

[2] A. Chao, *Physics of collective beam instabilities in high-energy accelerators*. 1993.

[3] G. Rumolo, "Beam Instabilities," no. arXiv:1601.05201, p. 21 p, 2014. Comments: 21 pages, contribution to the CAS - CERN Accelerator School: Advanced Accelerator Physics Course, Trondheim, Norway, 18-29 Aug 2013.

[4] E. Métral, X. Buffat, and G. Rumolo, "Transverse mode-coupling instability in the presence of detuning impedance," Apr 2020.

[5] N. Biancacci, E. Métral, and M. Migliorati, "Fast-slow mode coupling instability for coasting beams in the presence of detuning impedance," under publication.

[6] K. Li, H. Bartosik, S. Hegglin, G. Iadarola, A. Oeftiger, A. Passarelli, A. Romano, G. Rumolo, and M. Schenk, "Code development for collective effects," in *57th ICFA Advanced Beam Dynamics Workshop on High-Intensity and High-Brightness Hadron Beams*, p. WEAM3X01, 2016.

[7] https://github.com/PyCOMPLETE/PyHEADTAIL.

[8] https://gitlab.cern.ch/IRIS/SPS_IW_model/-/tree/master/SPS_IW_model_python.

[9] G. Iadarola, L. Mether, N. Mounet, and L. Sabato, "Linearized method for the study of transverse instabilities driven by electron clouds," *Phys. Rev. Accel. Beams*, vol. 23, p. 081002, Aug 2020.

[10] N. Mounet, "Vlasov Solvers and Macroparticle Simulations," *CERN Yellow Rep. Conf. Proc.*, vol. 1, pp. 77–85. 9 p, 2018.

[11] H. Burkhardt, G. Rumolo, and F. Zimmermann, "Coherent Beam Oscillations and Transverse Impedance in the SPS," Jun 2002.

[12] https://gitlab.cern.ch/jcoellod/harpy/-/blob/master/harmonic_analysis.py.

[13] A. Burov, "Efficiency of feedbacks for suppression of transverse instabilities of bunched beams," *Phys. Rev. Accel. Beams*, vol. 19, p. 084402, Aug 2016.

[14] C. Zannini, ""Benchmarking the SPS impedance model: Headtail growth rates." Presented at the CERN SPS Upgrade Working Group, 2014.

[15] https://github.com/ninad-sc/Multi-bunch-Tunes.

[16] G. Rumolo, "Extension of the two particle model to quadrupolar wakes." Presented at CERN HSC section meeting, Aug 2018.

A Machine Parameters

In all the simulations the machine used was the SPS at injection. Different optics were considered. The machine parameters are:

- Machine circumference = 6911 m
- Momentum compaction factor $\alpha = 0.00308$
- Lorentz factor $\gamma = 27.7$
- Beta function $\beta_x = \beta_y = 54.6$
- X tune $Q_x = 20.13$
- X tune $Q_y = 20.18$
- Synchrotron tune $Q_s = 0.017$
- Transverse emittances $\epsilon_x = \epsilon_y = 2 \times 10^{-6}$ m rad
- Bunch length $\sigma_z = 0.23$ m

B Impedance parameters

Three types of impedances were used. The first, a thick resistive wall has parameters:

- Pipe radius = 3 cm
- Resistive wall length = machine circumference
- conductivity = 10^6 S/m
- $dt_{min} = 10^{-3}/c$ s

The parameters of the broadband resonator were selected close to that seen in the actual SPS. They are:

- $R_{shunt} = 7$ MΩ
- frequency = 1 GHz
- Quality factor, Q = 1.

The wake table with single turn wakes was generated from the script available in the CERN impedance repository and used in the particle tracking simulations. For the analytical model, a 43 turn wake file from C. Zannini was used.